ROYAL SOCIETY
OF CHEMISTRY

PAPER

Check for updates

Tuning emissive color of trivalent terbium ion through environmental factors: optoelectronic insights from theoretical, spectral and computational studies†

Vandana Aggarwal,[a] Devender Singh, [ID] *[ab] Shri Bhagwan,[a] Raman Kumar Saini,[a] Komal Jakhar,[a] Sumit Kumar,[c] Parvin Kumar[d] and Jayant Sindhu[e]

The combination of 4,4,4-trifluoro-1-phenyl-1,3-butanedione (TFPB) and pyrazine (pyz) with Tb^{3+} ions forms two distinct types of complexes, represented by the formulas $[Tb(TFPB)_3(L)_2]$, where L is either H_2O or pyz, and $[(Tb(TFPB)_3)_2pyz]$. A detailed examination of the impact of the surrounding environment on the photophysical properties of these synthesized complexes was conducted. Photoluminescence (PL) analysis indicated that the magnetic dipole transition ($^5D_4 \rightarrow {}^7F_5$) is dominant in Tb(III)-based systems. The prepared complexes exhibit visible luminescence in both solid and solution media. Remarkably, the luminescence intensity of the mononuclear complex is significantly higher than that of its dinuclear counterpart, highlighting the impact of efficient energy transfer on emission intensity. The CIE color coordinates of these complexes in solution closely align with NTSC standard values. Additionally, modulation of emissive color is evident when the surrounding media (from solid to solution) and solvent nature are altered. Density Functional Theory (DFT) calculations were performed to elucidate the electronic density distribution in the synthesized complexes. Additionally, a comprehensive analysis, including IR, UV, NMR, thermogravimetry and cyclic voltammetry, was conducted, along with theoretical calculations using Judd−Ofelt analysis.

1. Introduction

The study of lanthanide-based complexes has gained significant attention in recent years due to their unique electronic configuration, which present them with intriguing optical[1] and magnetic properties. Among the trivalent lanthanide ions, terbium (Tb^{3+}) stands out as a remarkable ion owing to its distinct luminescent characteristics. This research investigates the synthesis and photophysical properties of mononuclear and dinuclear complexes featuring trivalent terbium ions. The complexes are designed with 1,3-diketone serving as the primary ligand and pyrazine as the neutral ligand, forming

novel complexes with promising optical attributes. The choice of ligands is crucial in determining the different properties of Ln-complexes. 1,3-diketones are known for their versatile coordination abilities, forming stable complexes with various metal ions.[2] Incorporating 1,3-diketone as the primary ligand aims to exploit its chelating capabilities, ensuring the formation of stable coordination compounds. Additionally, the inclusion of pyrazine as a neutral ligand introduces an aromatic, nitrogen-containing moiety, contributing to the structural diversity and potentially influencing the photophysical properties of the resulting complexes. Furthermore, this inclusion prevents the coordination of high-energy solvent moieties (O–H, N–H or C–H to a lower extent), enhancing luminescence intensity by reducing non-radiative relaxation of solvent oscillators.[3,4] Additonally, vast literature is already available involving lanthanide tris-β-diketonate luminescent complexes with neutral N-donor ligands.[5–12]

Trivalent lanthanide ions, characterized by partially filled 4f orbitals, exhibit unique electronic configurations that lead to distinctive luminescent properties.[13] Terbium, known for its green emission, provides an exciting platform for designing luminous materials for applications in optoelectronic devices, sensors[14] and biological imaging.[15,16] This study focuses on exploiting the luminescent potential of Tb^{3+} ions within novel

[a]Department of Chemistry, Maharshi Dayanand University, Rohtak-124001, Haryana, India. E-mail: devjakhar@gmail.com

[b]Department of Chemistry, Lovely Professional University, Phagwara, Jalandhar-144411, Punjab, India

[c]Department of Chemistry, DCR University of Science & Technology, Murthal-131039, Haryana, India

[d]Department of Chemistry, Kurukshetra University, Kurukshetra-136119, Haryana, India

[e]Department of Chemistry, COBS&H, CCS Haryana Agricultural University, Hisar-125004, Haryana, India

complexes. The coordination chemistry involving 1,3-diketone and pyrazine is explored, emphasizing the importance of ligand-to-metal ratios in achieving the desired structures. The structural aspects of the mononuclear and dinuclear complexes are thoroughly examined through various spectroscopic and analytical techniques, including thermogravimetry and IR, UV-vis, NMR and PL spectroscopy. Computational (DFT calculation) and theoretical (Judd–Ofelt analysis) studies are also performed on synthesized complexes. These studies aim to provide deeper insights into the bonding modes, redox behavior and thermal stability of the complexes along with their photoluminescent characteristics. Moreover, the influence of 1,3-diketone and pyrazine ligands upon electronic structure and photophysical properties of Tb^{3+} ions is also investigated. The main objective of this study is to analyze the photophysical features of the synthesized complexes. Luminescence studies, including emission and excitation spectra, luminescence lifetimes, branching ratio, intensity ratio and colorimetric parameters, are conducted to reveal the intricate details of the energy transfer processes within the complexes. The observed luminescent properties are correlated with the structural features of the complexes, providing a comprehensive understanding of the factors influencing their optical behavior. The insights obtained from this research hold promise for diverse applications across multiple domains, such as the development of luminescence components for various applications. Exploring the details of the photophysical features of Ln-complexes may prepare the way for designing tunable materials with enhanced functionalities. These investigations pave the way towards developing materials with advanced optical properties and a wide range of potential applications.

The primary aim behind this article is the formation of such Tb(III)-complexes that possess enhanced luminescence properties as compared to free Tb^{3+} ions. In this context, the focus of this study lies in the synthesis and in-depth characterization of three ternary terbium complexes based on a 1,3-diketone *i.e.* 4,4,4-trifluoro-1-phenyl-1,3-dione (TFPB) with pyrazine (pyz) as a neutral ligand. The selection of these ligands is inspired by their potential to tune the photophysical properties of Tb^{3+} complexes through ligand-field effects and energy transfer processes. In this article, two mononuclear eight-coordinated complexes of formula $[Tb(TFPB)_3(H_2O)_2]$ (TbA), $[Tb(TFPB)_3(pyz)_2]$ (TbM) and a dinuclear seven-coordinated complex with formula $[Tb_2(TFPB)_6(pyz)]$ (TbD) are prepared and abbreviated, as given in Table 1. In the former type of complexes, co-ligand *i.e.* pyrazine acted as a monodonor ligand and in latter type, it acted as a bridging ligand.

2. Materials

For synthesizing TbA, TbM and TbD, metal salt ($TbCl_3 \cdot 6H_2O$), TFPB and pyrazine were utilized. These chemicals were obtained from Sigma-Aldrich with chemical purities of 99.90%, 99% and ≥ 99%, respectively. Utilized solvents such as ethanol, hexane and 25% ammonia solution were SR/AR. No further purification or distillation was performed on the reagents and reactants before use.

3. Techniques

The CHN proportion of the prepared complexes was evaluated by a PerkinElmer 2400 Elemental Analyzer. Their IR transmittance spectra were collected in the form of KBr discs by falling mid-IR wavelength 400 cm^{-1} to 4000 cm^{-1} in a PerkinElmer 5700 FTIR Spectrometer. The Bruker Avance NMR II 400 spectrometer running at 400 MHz was employed to record proton magnetic resonance signals. Here, TMS and $CDCl_3$ were utilized as reference and solvent, respectively. The absorption spectra of the formed complexes, along with TFPB, were recorded using a Shimadzu 2450 UV-visible spectrophotometer in both solid and solvated forms, with DCM (dichloromethane) and DMSO (dimethyl sulfoxide) as solvents. The instrument is equipped with two energy sources: a hydrogen discharge lamp for the UV region (150–400 nm) and a tungsten filament lamp for the visible region (400–700 nm). In order to obtain the solid-state UV-vis absorption spectra, the sample solid is powdered and pressed into a suitable holder to create a flat surface for analysis. Barium sulfate ($BaSO_4$) was used as a reference material to correct for background scattering effects. Instrument was then calibrated using the reference material. Subsequently, powdered solid sample (2×10^{-5} moles) was carefully placed into the sample holder over the reference material at the center. Then, spectrophotometry was performed across 200–800 nm range, recording the absorbed light intensity at each wavelength. Finally, obtained data is analyzed. For obtaining solution-state UV absorption spectra, sample solutions with concentrations 10^{-5} M were prepared using an appropriate solvent. Calibration of the spectrophotometer was performed using pure solvent in both cuvettes. Quartz cuvettes, which do not absorb in the UV range, were used for all measurements. A Horiba Jobin YVON Fluorolog FL-3–11 Spectrophotometer was used to record the photoluminescent excitation and emission profiles of these comlexes in powder and solvated phase utilizing a non-coordinating (DCM) and a coordinating (DMSO) solvent. Decay times of the most stable emitting state of these complexes were recorded on an F-7000 FL Spectrophotometer at

Table 1 Percentage (%) CHN assessment (exp. and theor.) of TbA–TbD

Complex	Color	$C_{exp.}$ (theor.)	$H_{exp.}$ (theor.)	$N_{exp.}$ (theor.)	Formula
TbA	Wheatish	42.87 (42.86)	2.64 (2.59)	—	$C_{30}H_{22}TbF_9O_8$
TbM	Wheatish	47.32 (47.36)	2.72 (2.69)	5.81 (5.74)	$C_{38}H_{26}TbF_9N_4O_6$
TbD	Wheatish	45.52 (45.48)	2.39 (2.47)	1.66 (1.57)	$C_{64}H_{40}Tb_2F_{18}N_2O_{12}$

20 ms scan rate. The chromaticity color coordinates were determined by putting photoluminescence emission data in use with the help of Color Calculator. A Potentiostat 4000 was used to evaluate electrochemical spectra (cyclovoltammograms) at a scan rate of 10^{-1} V s^{-1}. Three electrode system consisting of glassy carbon, platinum and silver electrode was used for analysis of CV curves. The cyclic electrochemical curves were recorded in DCM solvent with a 10^{-1} M NBu$_4$ClO$_4$ as supporting electrolyte. The thermogravimetric patterns were captured on a Hitachi STA-7300 instrument at a heating rate of 10 °C min^{-1} in N$_2$ atmosphere.

4. Synthesis

4.1 [Tb(TFPB)$_3$(H$_2$O)$_2$]

An adequate amount of ligand TFPB (0.6 mmol) was dissolved in 5 mL ethanol and was deprotonated with an equivalent molar quantity of ammonium hydroxide solution (0.6 mmol). The mixture was left undisturbed for a few hours until the essence of ammonia completely quenched. TbCl$_3$·6H$_2$O (0.2 mmol) was dissolved in 5 mL ethanol to form an ethanolic solution of the metal salt. Subsequently, this ethanolic solution was added slowly and dropwise to the previously prepared solution of the ammonium salt and the resulting mixture was left to stir for around 12 h at RT. After the stirring period, the mixture was left to slowly evaporate for 2–3 days during which precipitates were formed. The obtained precipitates were filtered off and rinsed with distilled water and hexane to eliminate impurities from the formed complexes. Afterwards, precipitates were left to dry in oven over P$_4$O$_{10}$ (Fig. 1).[17]

4.2 [Tb(TFPB)$_3$(pyz)$_2$]

These complexes were prepared in the same way as mentioned above. The only difference being that an ethanolic solution of pyrazine was prepared by dissolving 0.4 mmol of pyrazine in 5 mL ethanol. Subsequently, the ethanolic solution of both metal salt and neutral ligand were added slowly and dropwise to the previously prepared solution of the ammonium salt and the resulting mixture was treated with the same procedure as detailed above. The obtained precipitates were filtered off and washed with ethanol and hexane to eliminate impurities from the prepared complexes. Afterwards, the precipitates were left to dry in oven over P$_4$O$_{10}$ (Fig. 2).[18–20]

4.3 [(Tb(TFPB)$_3$)$_2$pyz]

For synthesizing [(Tb(TFPB)$_3$)$_2$(pyz)], the precipitates of complex [Tb(TFPB)$_3$(H$_2$O)$_2$] were dissolved in adequate amount of ethanol. In a separate step, an ethanolic solution of pyz (0.10 mmol) was prepared i.e. these formerly prepared chelates were made to react with pyz in 2 : 1 molar ratio in C$_2$H$_5$OH. Subsequently, these two solutions were mixed at 50 °C and stirred continuously for about 12 h. Then, similar procedure was followed as mentioned in 1st and 2nd synthetic route. This lead to the formation of a new seven-coordinated dinuclear complex [(Tb(TFPB)$_3$)$_2$(pyz)] (Fig. 3).[21,22] All the three prepared complexes were thoroughly characterized via various spectroscopic and analytical procedures.

5. Results and interpretation

5.1 CHN analysis

The prepared Tb(III) ion centered mononuclear and dinuclear complexes were wheatish in color. Their chemical formulas were determined based on CHN analysis results, which are in agreement with theoretical predictions. The calculated differences are within the range of 0.03–0.09 affirming the accuracy of the results. Table 1 presents the experimental (exp.) and theoretical (theor.) percentages of C, H and N for each complex, along with their respective colors, suggested formulae and
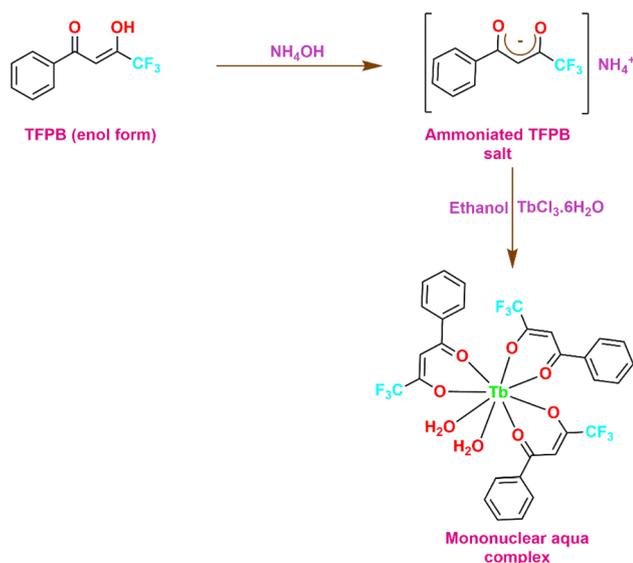

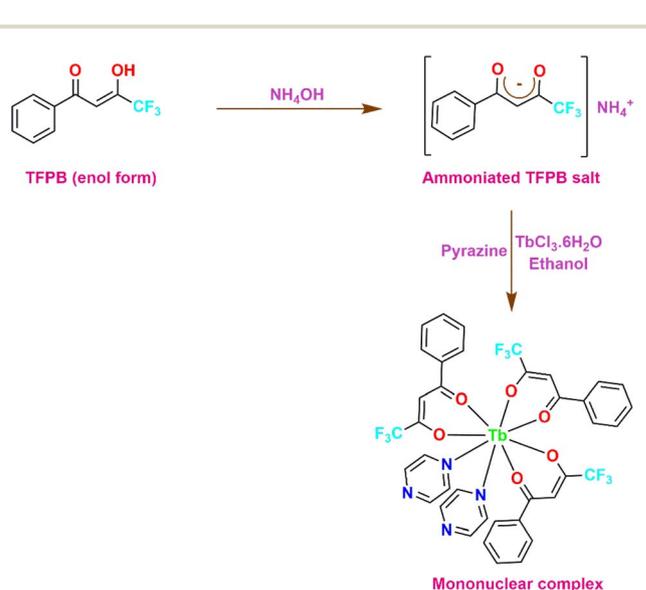Fig. 1 Synthetic scheme for synthesizing mononuclear aqua complex (TbA).

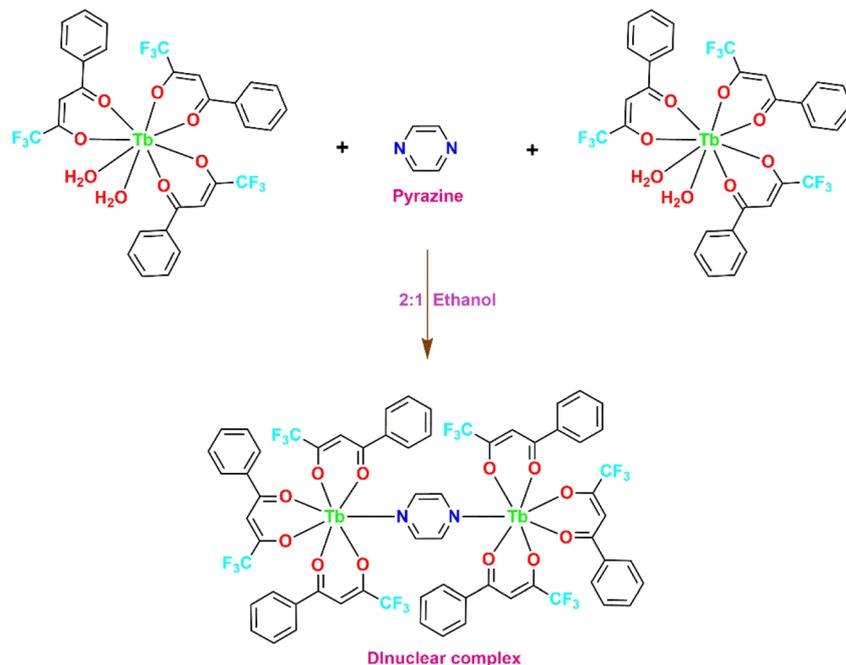Fig. 2 Synthetic scheme for synthesizing TbM.

Fig. 3 Synthetic scheme for synthesizing TbD.

abbreviated names for convenient reference throughout the text.

5.2 IR study

The IR technique was utilized to assign the observed peaks and bands to the functional groups of both uncoordinated ligands and any shifts in the vibrational frequency that might indicate bonding with the trivalent ion in complexes. Fig. S1–S3† display the obtained FT-IR profiles of TbA–TbD, respectively. Table 2 summarizes the key spectral peaks characteristic of the coordinated and uncoordinated ligands (TFPB and pyz). It is observed that the peaks related to complexes showed a red-shift compared to those of uncoordinated ligands, suggesting bonding with the Ln^{3+} ion.[23] Additionally, peaks near 580 cm^{-1} and 459 cm^{-1} are accredited to the M–N and M–O bond stretches, respectively, in pyrazine based complexes.[24] For TbA, the M–O bond stretch occurs at 460 cm^{-1}. The IR spectral data displayed a significant shift in the C═O bond stretch frequency of diketonic moiety. This stretching in free TFPB appears at ∼1604.5 cm^{-1} and shifts to 1598 cm^{-1} after complexation,

indicating coordination to trivalent ion.[25] The broad band corresponding to (symm.) symmetric and (asymm.) asymmetric O–H stretching in TbA confirms the presence of coordinated water molecules in this complex. Absence of this band in TbM and TbD indicates coordination of pyrazine moieties with Ln^{3+} ion, replacing water moieties and suggesting diketone coordination with metal ion *via* O-atom.

Prepared complexes exhibit strong peaks around 1467 cm^{-1} due to C═C stretch and pyrazine-coordinated complexes (TbM and TbD) show a peak around 1530 cm^{-1} attributed to C═N stretching vibrations.[26] IR spectrum of ternary 1,3-diketonate complex demonstrates enolic ═CH (3050 cm^{-1}) and C–N (1320 cm^{-1}) vibrational modes, while for binary complex TbA, ═CH stretch appears at ∼2900 cm^{-1}.[27] C–F band is relocated to a lower wavenumber *i.e.* 1141 cm^{-1} (symm.) and 1181 cm^{-1} (asymm.) in the recorded IR spectra of the mono and binuclear complexes, indicating complex formation.[28] The majority of IR peaks and bands originating from free pyz are masked by the robust IR absorptions of TFPB, making it difficult to observe its characteristic peaks and bands in TbM and TbD. A peak at 1457 cm^{-1} in free pyz is shifted to 1435–1438 cm^{-1}. When pyrazine coordinates through a single nitrogen atom, as in complex TbM, a band emerges between 940 and 1010 cm^{-1} due to reduced molecular symmetry faced by pyz. TbM exhibits a band at 944 cm^{-1}, distinct from its counterparts in the IR spectrum of TbD, indicating the coordination of pyrazine moieties through only one of their nitrogen atoms.

5.3 H NMR spectroscopy

Proton magnetic resonance spectroscopy was performed to confirm the formation of expected mono and dinuclear

Table 2 IR data of ligands and prepared complexes (in cm^{-1})

Compound	TFPB	pyz	TbA	TbM	TbD
$v_{(Ln–O)}$	—	—	460	459	461
$v_{(Ln–N)}$	—	—	—	580	581
$v_{(C–F)}$	—	—	1141, 1186	1143, 1187	1141, 1189
$v_{(C–N)}$	—	—	—	1320	1321
$v_{(C═C)}$	—	1457	1465	1438, 1467	1437, 1466
$v_{(C═N)}$	—	—	—	1533	1533
$v_{(C═O)}$	1604.5	—	1598	1598	1598
$v_{(═CH)}$	—	—	2927	3137	2928

Table 3 Proton chemical shifts (in ppm) of TbA–TbD

Complex	Peaks of TFPB	Peaks of pyz
Free ligand	5.982 (1H), 7.516 (2H), 7.547 (2H), 7.864 (1H), 14.6 (1H)	8.50 (4H)
TbA	108.28 (s), 7.29–7.56 (m)	1.57 (s)
TbM	116.13 (s), 7.17–7.85 (m)	−32.15 (s), −198.45 (s)
TbD	145.08 (s), 7.22–8.02 (m)	−191.88 (m)

complexes TbA, TbM and TbD (Fig. S4–S6,† respectively). The spectra were recorded using deuterated chloroform (5 × 10⁻² M) as the solvent. The results are consistent with the presence of single and dual metal centers in (TbA, TbM) and (TbD), respectively (Table 3). The spectra showed distinct features: free pyrazine displayed a sharp singlet at 8.50 ppm,[29] while TFPB signals appeared at chemical shifts (in ppm) 14.6, 7.86, 7.54, 7.52 and 5.98 corresponding to O–H proton, three signals of phenyl group and for methine proton, respectively.[30] Complex TbM exhibited two line-like peaks of equal intensity for pyrazine protons at −32.15 and −198.45 ppm, respectively. Protons near the ion exhibited higher upfield shifts (even up to negative values) compared to the distant protons. The presence of two resonances of equal intensity for pyrazine protons confirmed bonding *via* a single N-site to the metal ion. The coordination of two pyrazines with Tb³⁺ ions, along with three TFPB units, is confirmed by the intensity ratio of protons between TFPB and pyrazine. This ratio of proton signals corresponding to primary and secondary ligands supports the eight-coordinated behavior of metal center. Noteworthy observations include shifts towards higher δ values for methine protons in the TbM complex compared to free TFPB and significant shifts towards higher and lower δ values for TFPB and pyrazine protons, respectively. The dipolar nature of the paramagnetic shift is evidenced by shifts in opposite directions for TFPB and pyrazine protons in both complexes as given by the eqn (1).[31,32]

$$\Delta_p = D_1 \left(\frac{3\cos^2\theta - 1}{r^3} \right) \quad (1)$$

Herein, all the symbols have their standard meanings. The paramagnetic shift's magnitude varies inversely with the distance between paramagnetic metal ion and the proton, resulting in larger shifts for protons closer to metal ion. PMR spectra of complex TbD displayed three signals, confirming the coordination of one pyrazine to two [Tb(TFPB)₃] units, resulting in a seven-coordinate Tb(III) ion. Proton resonances of TFPB experienced shifts in opposite directions to that of pyz protons, providing strong evidence of the predominantly dipolar nature of the paramagnetic shift in these complexes. Complex TbA displayed three signals: two due to TFPB (a sharp singlet for three methine protons along with a multiplet due to 15 aryl protons in 7.10–8.00 ppm range) and one signal due to coordinated water molecules.

5.4 UV analysis

The optical absorption characteristics of the synthesized complexes were collected in both solid and liquid phases at a 5 mM concentration, using DCM as a non-coordinating solvent and DMSO as a coordinating solvent. Pyrazine exhibits strong UV absorption between 200 and 275 nm, with the maxima ~250 nm and a shoulder band near 306 nm.[33] Furthermore, the diketone TFPB strongly absorbs UV radiation in the range of 200–400 nm with maxima at 314 nm.[34] All the complexes give similar UV profiles across different medium thus, only the spectra in DCM solvent are presented here (Fig. 4 and Table 4). Spectra for solid and liquid (DMSO) samples are provided in ESI file (Fig. S7 and S8).† The spectral absorption profiles of TbA feature two bands in region 250–370 nm corresponding to S₀ → S₁ transition of bonded 1,3-diketonate (TFPB), whereas TbM and TbD complexes show a wide and strong band ranging from 290 to 375 nm in UV region of electromagnetic spectrum. This band is attributed to S₀ → S₁ transition corresponding to π–π* levels of bonded 1,3-diketonate (TFPB) and pyrazine moieties.[35] The UV-absorption profiles of prepared compounds align well with that of uncoordinated moieties, showing a bathochromic shift (nephelauxetic effect) relative to them. This effect could be attributed to the perturbation induced by the coordination of metal ion with ligands.[36] TbM and TbD complexes exhibited a prominent band around 324 nm despite of changing the nuclearity of the complex. This is possibly due to the presence of same absorbing moieties *i.e.* TFPB and pyrazine in these complexes. No shift in band position or any change in band shape shows that the aforementioned moieties are the primary absorbers of incident UV radiation and metal ion does not itself absorb much of the
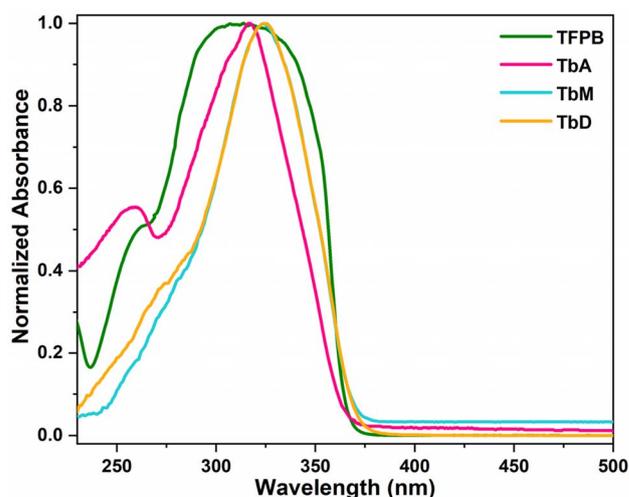

Fig. 4 Normalized UV-vis profiles of TFPB and synthesized complexes.

Table 4 Various photosensitive features of TbA–TbD

Compound	λ_{abs} (nm)	E_g (eV)	λ_{ex} (nm)	λ_{em} (nm)	Lifetime (ms)
TbA	317	3.501	367	553	0.103
TbM	324	3.425	371	545	0.466
TbD	324	3.413	369	545	0.366

incident UV rays. Moreover, no intraconfigurational f–f transitions are appeared in UV-visible range of the absorption spectra.[37]

5.4.1 Band gap analysis. The coordination of a metal ion with the spacer ligand not only meets its high coordination requirement, but it also increases coordination saturation and thermal stabilities of dinuclear complexes.[38] The optical band gap (E_g) values (Table 4) of synthesized compounds were obtained by putting UV-absorption data into Tauc's equation (eqn (2)).[39,40]

$$\alpha h\nu = A(h\nu - E_g)^n \qquad (2)$$

where, α represents molar absorption constant, $h\nu$ identifies energy, A denotes electronic tailing coefficient and n indicates

optical component (indirect/direct). To estimate band gap E_g, the plot of $(\alpha h\nu)^2$ *versus* energy ($h\nu$) is constructed using Tauc plot and a tangent is drawn to the x-axis until $y = 0$. Table 4 presents the obtained E_g data while Fig. 5 depicts their respective curves.

5.5 Photoluminescence spectroscopy

The PL excitation and emission spectra of all the complexes were recorded in solid and solution phase ($c = 1 \times 10^{-5}$ M) for which two different solvents were used. Out of which, one is non-coordinating (DCM) and other is coordinating (DMSO), in order to observe their influence on the luminous characteristics of complexes. Fig. 6 and 7 represent the excitation and emission spectral profiles of the synthesized complexes in solid and liquid form (DCM and DMSO).

5.5.1 [Tb(TFPB)$_3$(H$_2$O)$_2$] (TbA), [Tb(TFPB)$_3$(pyz)$_2$] (TbM) and [(Tb(TFPB)$_3$)$_2$pyz] (TbD). The optical excitation spectra of Tb(III) complexes were obtained by adjusting the emission wavelength (λ_{em}) at 545 nm. The corresponding spectra display a very strong band due to $S_0 \rightarrow S_1$ transition within π molecular orbitals of antenna ligands. This high intensity band is accompanied by a less intense transition from ($^7F_6$) ground state of Tb^{3+} ion to ($^5L_9$) excited state at ~361 nm in solution
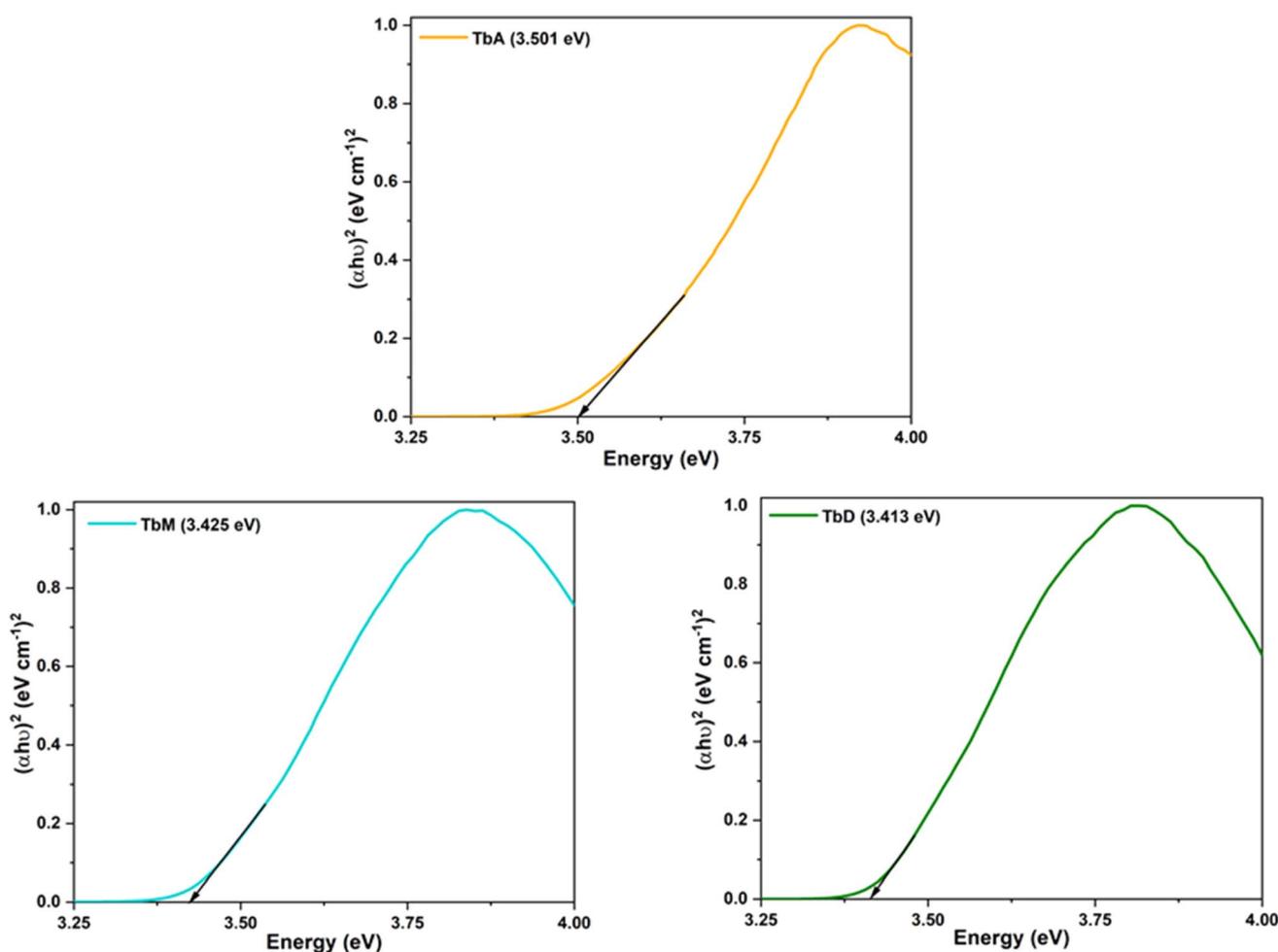

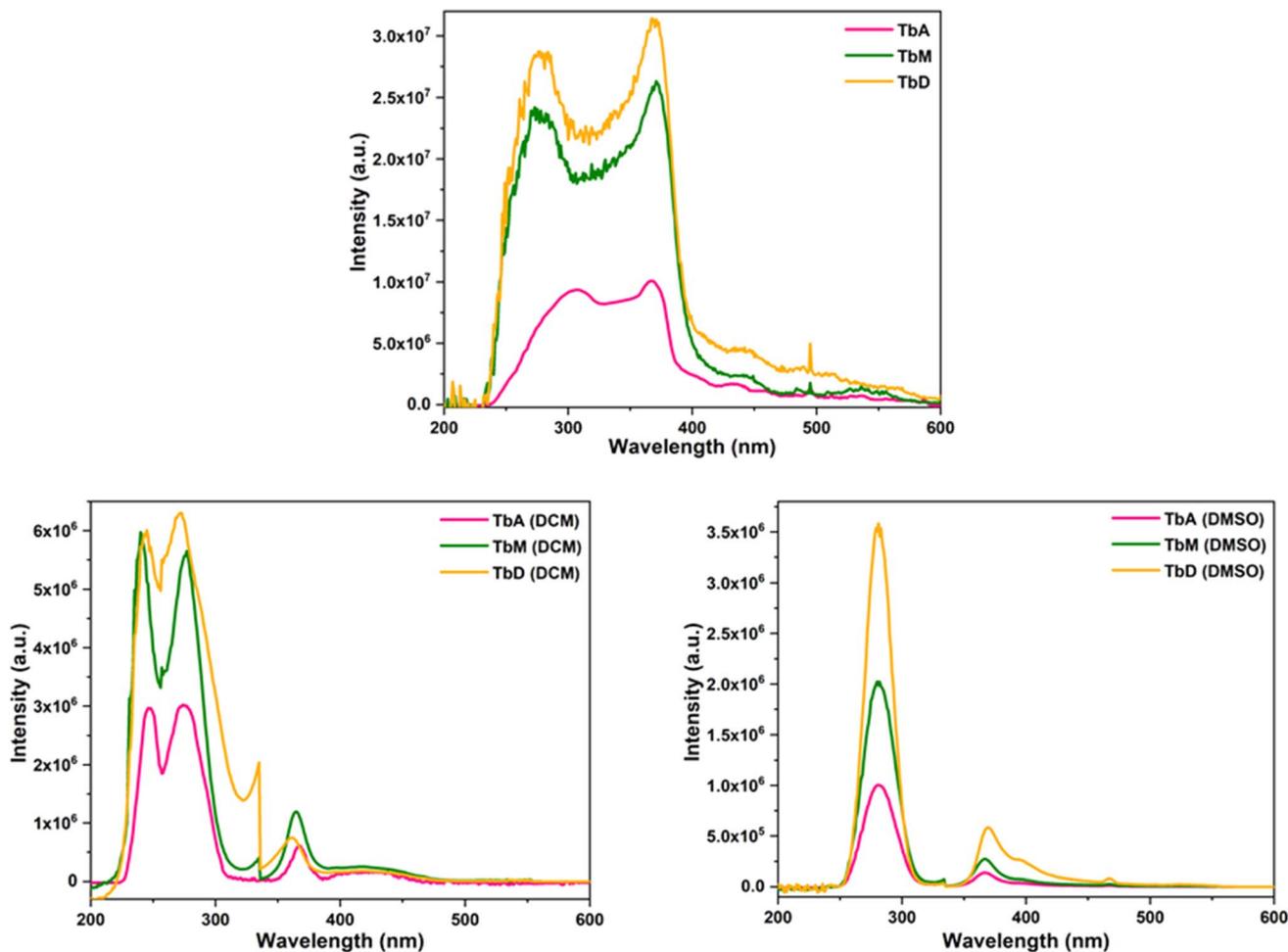**Fig. 5** Bandgap profiles of synthesized complexes.

Fig. 6 Excitation profiles of TbA, TbM and TbD in solid and solution form (DCM and DMSO).

media.[41] The band maxima of this band for TbA, TbM and TbD is noted at 367, 371 and 369 nm (solid); 274, 276 and 272 nm (DCM); and 281, 281 and 281 nm (DMSO), respectively. Spectral profiles of all the complexes display similar shapes of different intensities owing to the number of absorbing moieties. A large difference in excitation wavelengths between the solid (∼370 nm) and liquid states (∼275 and 281 nm) of the complexes is observed. This can be attributed to various factors associated with surrounding environment and solvent interactions in the case of the liquid state, compared to the solid-state packing in the case of the solid state which influences the electronic structure and the energy levels within the complexes.

The photoluminescence emission spectra exhibits four peaks due to $^5D_4 \rightarrow {}^7F_j$ transitions where j = 6, 5, 4, 3 at 492 nm, 544 nm, 586 nm and 613 nm, respectively.[42] The transition $^5D_4 \rightarrow {}^7F_6$ transition is electrically dipole and is hypersensitive to the coordinating environment.[43] The ΔJ = +1 transition is observed to be the most intense transition and found to be magnetically dipole in nature.[44] This transition exhibited stark splitting and is primarily responsible for their green emission. The energy of triplet state of employed diketone (TFPB) is 21 600 cm^{-1} (ref. 45) which lies above the emitting state of Tb(III)

ion having energy of 20 325 cm^{-1} (ref. 46) (Table 5). But this difference (1275 cm^{-1}) might be not sufficiently ideal for an effective transfer of energy from TFPB towards Tb(III) ion to take place. It is important to highlight that the intensity of hyperintense transition $^5D_4 \rightarrow {}^7F_5$ of Tb(III) ion-centered complex is multi-folds higher in solid state than that of solution phase. It is approximately 6 and 18 folds intensified as compared to the intensity of this transition in DCM and DMSO, respectively. This can be credited to the faster radiationless relaxations in the solvated form than solid phase which results in lesser luminescence intensity. The intensity in DMSO is found to be lower in comparison to DCM which could be attributed to the coordinating nature of DMSO. Along with the metal based peaks, ligand-based broad band are also noted in the emission profiles of these complexes in both media. This observation is an evidence for inefficient sensitization of metal center *via* ligands as these ligands itself show radiative relaxation. The asymmetry ratio (η) of electric dipole to magnetic dipole transition *i.e.* in different environment for TbM is 0.29 (solid), 2.18 (DCM) and 0.45 (DMSO). Similar results are observed for complex TbD [0.29 (solid), 1.18 (DCM) and 0.53 (DMSO)] and for TbA. The higher values are indicative of strongly polarizable environment in the
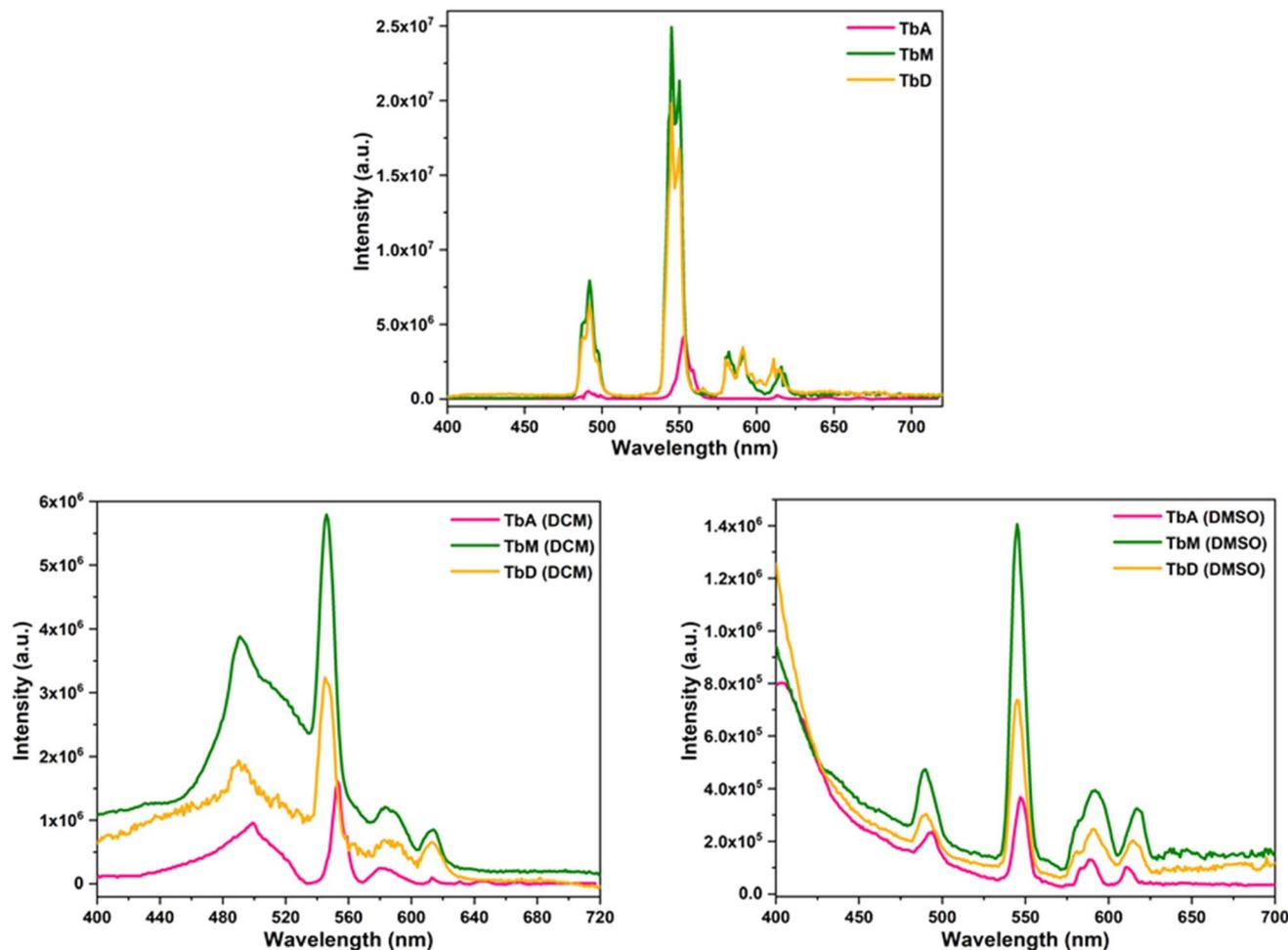
Fig. 7 Emission profiles of TbA, TbM and TbD in solid and solution form (DCM and DMSO).

Table 5 Triplet state (T_1) energy along with their difference with emitting state of metal ion

Compound	Energy (cm^{-1})
E_{pyz}	26 820 (ref. 47)
E_{TFPB}	21 600
$E_{Tb(III)}$	20 325
$\Delta E_{TFPB-Tb(III)}$	1275
$\Delta E_{Pyz-Tb(III)}$	6495

DCM phase. Spectra of all the complexes revealed similar shapes which can be easily seen from the extent of their overlapping but the intensity of TbD is found to be lower than TbM. This could be attributed to the number of pyrazine ligands attached to the metal center for the energy transfer to the concerned metal ion. Hence, the metal center is relatively less sensitized in dinuclear complex (TbD) here, than in mononuclear complex (TbM). Moreover, the spectra of TbA presents less emission intensity owing to the presence of high energy O–H oscillators within the coordination sphere which act as luminescence quenchers.

5.5.2 Solvent influence. The strength of electric dipole transition in Tb^{3+} complexes is significantly affected by the surrounding coordination environment of the ions and varies with the dissolving medium.[47] Interestingly, the emission lines exhibit greater intensity in DCM – a non-coordinating solvent compared to DMSO – coordinating solvent as shown in Fig. 7. Specifically, the intensity of hyper-intense transition $^5D_4 \rightarrow {}^7F_5$ for Tb^{3+} ion is higher in DCM than in DMSO. The intensity parameter (η), which indicates the polarizing capacity of the surrounding environment around Ln^{3+} ions, also changes with the medium. For the Tb^{3+} complexes presented, η values are higher in DCM solvent than in the powder phase and DMSO. The comparatively lower emission intensity in coordinating solvents is mainly due to the resonance between the 1st vibrational overtone of the solvent oscillators and smaller energy gap among the emitting level and subsequent lower energy level of metal ion.[48] Additionally, dipole–dipole interaction between the coordinating moieties (TFPB and pyz) and the solvent molecules can lead to quenching of the T_1 level.[48] The hypersensitive transition for metal ion displays stark splitting in solid phase, whereas this transition remains unified without splitting in the solution form. This stark splitting indicates a higher

asymmetric environment around the metal ion in solid phase.[49] The higher non-symmetric coordination environment around Tb^{3+} ion tends to enhance the emission intensity and similar results are observed *via* PL spectral analysis. The reduced luminescence intensity in solution-complexes might be attributed to solvent vibrations, which effectively quench luminescence *via* non-radiative relaxation mechanisms. Additionally, in solution-phase, solvent effects including polarity, hydrogen bonding and solvation, can alter the energy levels of the complex and lead to shifts towards longer or shorter wavelengths in the excitation spectrum. Whereas, in the solid state, the molecular packing, crystal field effects and intermolecular interactions can shift the excitation wavelengths in a different direction compared to the liquid state. Therefore, the large difference in excitation wavelengths could be primarily due to the different physical environments in which the material exists in the solid *versus* liquid states, leading to variations in the electronic structure and interactions.

5.5.3 Emission mechanism. The intramolecular energy transfer is the critical process which contributes to the luminescent behaviour of ternary Tb(III) complexes (TbA–TbD). The two core hypothesis *i.e.* Dexter and Förster are associated with the triplet level (T_l) of organic chromophore and energy of emitting level of Ln(III) ion for intra molecular energy transfer process. An optimal energy difference is a prerequisite for an efficient energy transfer to take place between these energy levels. Emitting state $^5D_4$ of Tb(III) ion is positioned at 20 325 cm^{-1}.[46] However, the T_1 levels of ligands are 21 600 cm^{-1} (TFPB)[45] and 26 820 cm^{-1} (pyz).[50] The energy gap (ΔE) among emitting state of Tb(III) ion *i.e.* $^5D_4$ and T_1 level of chromophores are 1275 cm^{-1} (TFPB), 6495 cm^{-1} (pyz). The strong luminescent emissions observed in these complexes suggest that the organic moieties employed in this study exhibit high energy transfer efficiency. Although it is well reported in literature the optimum energy gap of 1850–2250 cm^{-1} is for most efficient energy transfer from donor to acceptor which in turn leads to highest luminescence intensity. However, $\Delta E_{(Tb(III)-TFPB)}$ is significantly lower and $\Delta E_{(Tb(III)-pyz)}$ is significantly higher than the above mentioned range. Consequently, back-transfer of energy is expected from acceptor to donor moiety resulting in broad ligand-based band in emission profile, as observed in solid state emission spectra of TbA–TbD. This observation suggests that
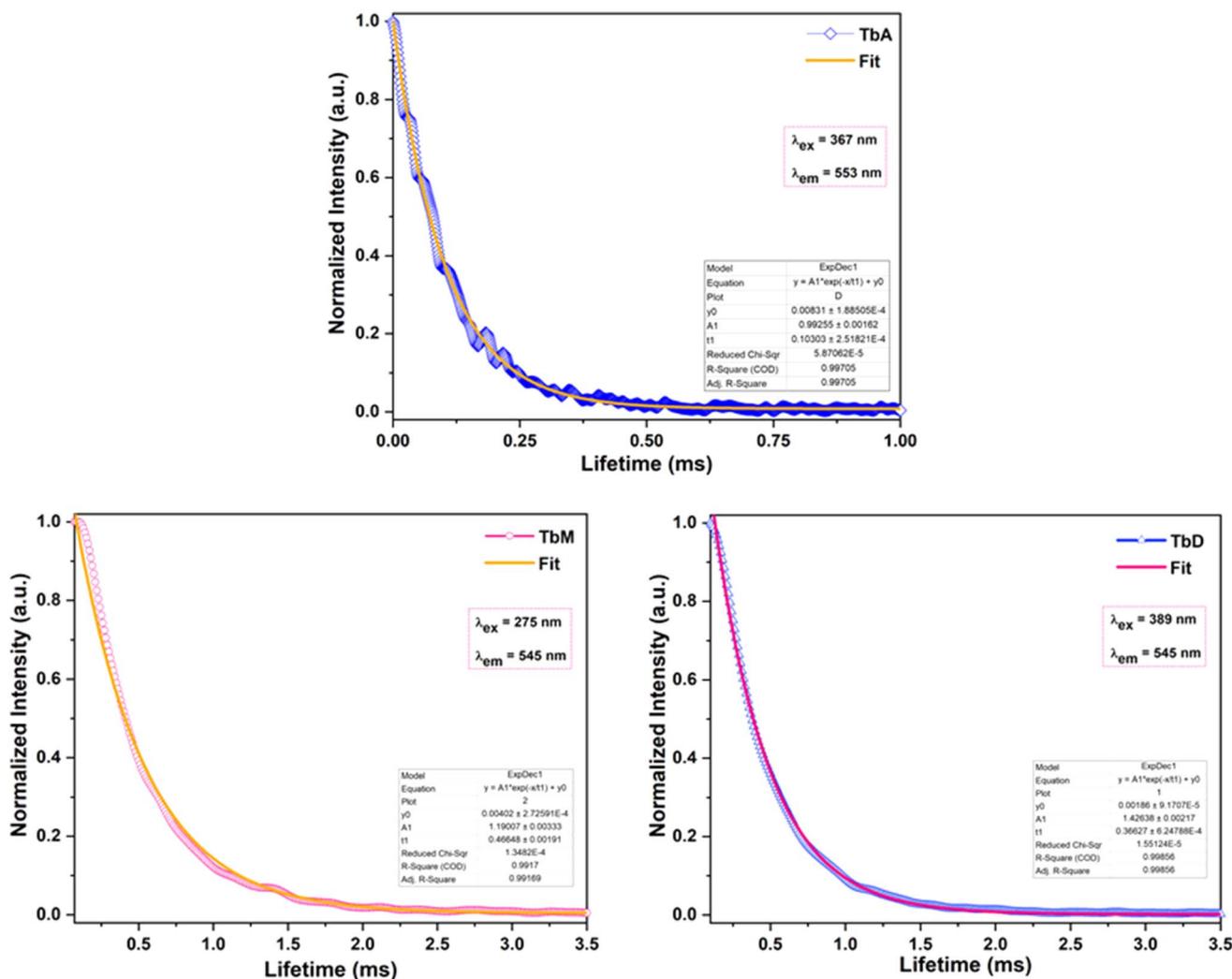

Fig. 8 Decay time-profiles of TbA–TbD.

energy is inefficiently transferred from attached chromophores to the Tb(III) ion leading to observed emission intensity in PL profiles. Nevertheless, the luminescence intensity of TbM was found higher than TbD. This could be credited to the number of pyrazine molecules coordinated to the metal ion (one in TbD and two in TbM). This observation also suggests that pyrazine

Table 6 Color coordinates of TbA–TbD

Complex	TbA			TbM			TbD		
Medium	Solid	DCM	DMSO	Solid	DCM	DMSO	Solid	DCM	DMSO
x, y	0.325, 0.614	0.213, 0.377	0.221, 0.195	0.354, 0.571	0.319, 0.317	0.263, 0.400	0.403, 0.502	0.267, 0.352	0.305, 0.268
u', v'	0.134, 0.568	0.120, 0.478	0.180, 0.358	0.154, 0.562	0.436, 0.519	0.142, 0.498	0.196, 0.550	0.159, 0.473	0.217, 0.430
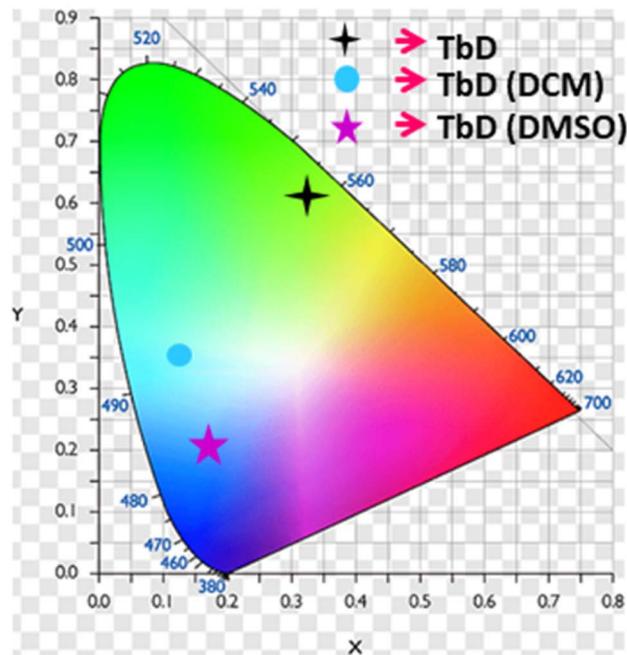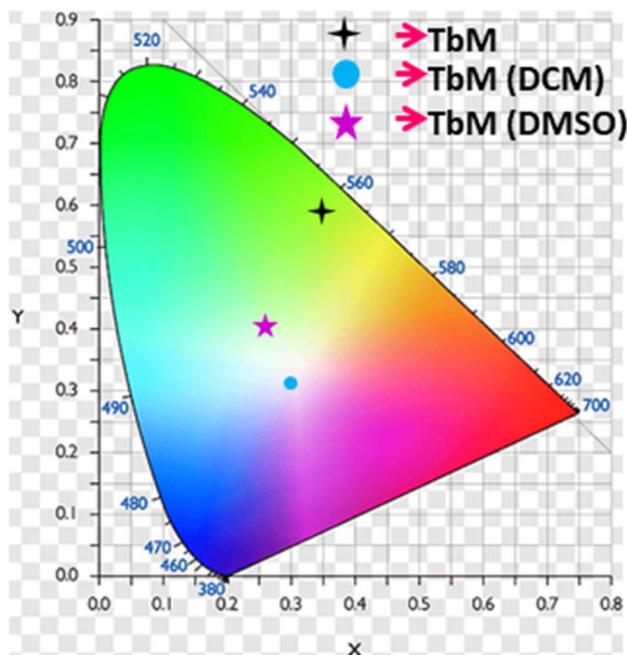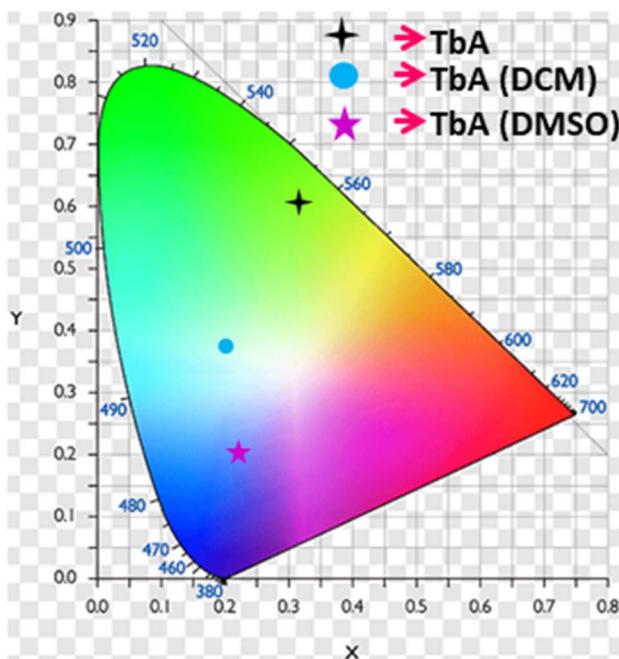
Fig. 9 (x, y) Coordinates of TbA, TbM and TbD in both solid and solution form (DCM and DMSO).

acted as comparatively more efficient sensitizer than TFPB itself. TbA displayed least emission intensity owing to the presence of water molecules (high energy O–H oscillators) in the first coordination sphere which leads to quenching. Similar observations were made from emission spectra of these complexes in solution phase. However, a decrease in the intensity of the peaks with peak broadening is observed along with high and broad ligand-based band upon solvating these complexes in DCM and DMSO. This decreased intensity with broad peaks and ligand based band is even more pronounced in DMSO as compared to DCM owing to its coordinating behaviour.

5.5.4   Decay time. The duration of fluorescence deactivation is a critical parameter for practical applications of luminescence, such as FRET (Florescence Resonance Energy Transfer).[51] In this article, the emission decay profiles of the synthesized complexes were determined using time-resolved luminescence analysis at their respective excitation and emission wavelengths in the solid form at RT. Fig. 8 clearly illustrates that decay profiles of emitting level of Tb(III) ion ($^5D_4$) are best fitted by a single-exponential function. The decay lifetimes of TbA, TbM and TbD in solid phase are determined to be 0.103 ms, 0.466 ms and 0.366 ms, respectively. PL decay time refers to the mean time a molecule remains in its most stable excited state before emitting a photon, resulting in luminescence.[52] Usually, the decay profiles of the emitting level of Ln^{3+} ion are best fitted by a single-exponential function, indicating either the presence of a single emitting ion in the system or multiple ions in similar sites with comparable coordination environments, each exhibiting similar lifetimes. Mono-exponential function is expressed by eqn (3):[53]

$$T(t) = I_0 + A_1 \exp(-t/\tau) \qquad (3)$$

Where, A_1 is quantity acquired from fitting, $I_0 = 0$, t = time in ms and τ is decay lifetime for mono-exponential fit. These numerical data denotes the presence of mono-chemical

environment for the emitting Tb(III) ion and the results of absorption and PL investigations are presented in Table 4.

5.5.5   Color tuning. The emissive color of prepared complexes is determined by chromaticity functions which are three-unitless parameters in Commission Internationale de l'Éclairage CIE 1931 color coordinate framework. These functions are used to calculate x, y chromaticity coordinates, as shown in Table 6. CIE diagrams (Fig. 9) based on the PL spectra reveal distinct colors for prepared complexes in various phases. Analysis of the CIE color triangle indicates that the complexes exhibit color variation depending on the phase. The intensity and wavelength of emission from these complexes changed significantly *i.e.* residual fluorescence (I_B), increases in solution media (Fig. 7). The tuning of terbium complexes' emission colors is observed, with the ability to shift from green to white, blue and pink in TbA, TbM and TbD, based on different energy transfer pathways (Table 6). In instances of higher energy absorption, the antenna effect predominates, resulting in an intense-green color for Tb(III) complexes in the solid state (Fig. 9). Conversely, when absorbed energy is insufficient for efficient intersystem crossing, I_B dominates in blue region, leading to white, pink and blue colors for TbA, TbM and TbD, respectively in solution form. CIE diagrams in Fig. 9 visually demonstrate the color changes with variations in the medium. By carefully adjusting the relative intensity of green emission (I_A) of Tb(III) complexes and blue emission (residual fluorescence/I_B) across various phases in PL spectra of these Tb-complexes, modulation of emissive color can possibly be achieved, offering a potential approach for white light emission.[54] This suggests that working with such materials holds promise for fabricating WLE (white light-emitting)-devices or RGB-emissive components to be utilized in photonic appliances. Additionally, the emission colors encompassing nearly full range of visible wavelengths in different phases makes these complexes suitable as color indicators.[54]

5.5.6   Judd–Ofelt calculation. Judd–Ofelt theory (J–O theory) is a conceptual approach which provides understanding
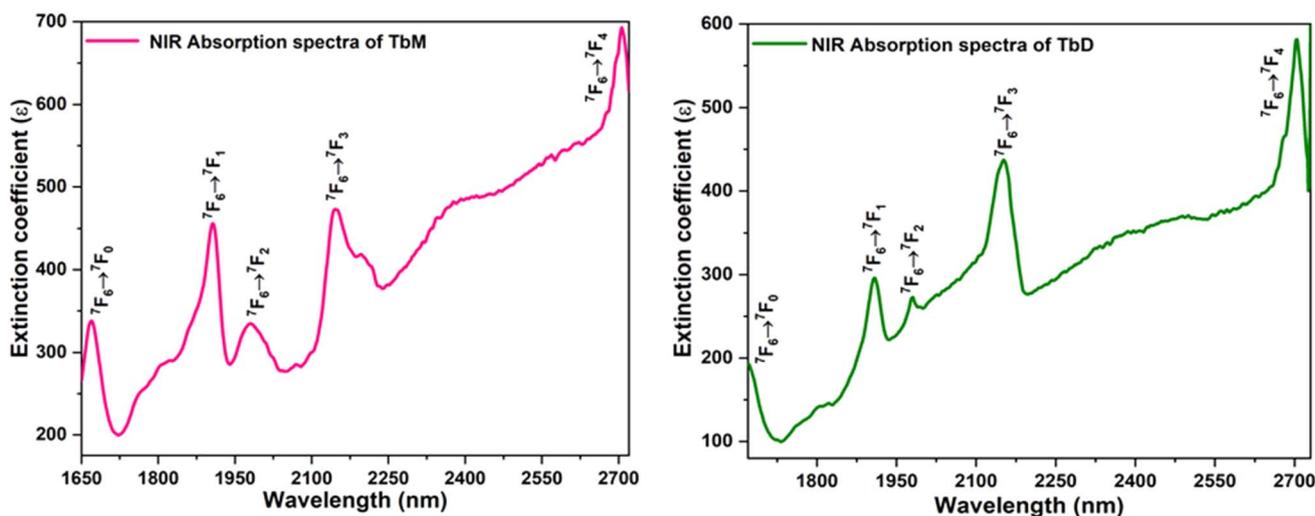

Fig. 10   NIR absorption spectra of TbM and TbD.

regarding the photoluminescence properties of Ln^{3+} ion in solid state. It provides quantitative insights of the effect of coordinating environment on emissive transitions of Ln ions. Basically, this theory assumes that crystal field interaction exists between Ln^{3+} ion and donor ligands and the transitions between various energy levels of Ln ions are primarily dipole allowed.[55] Based on these assumptions, J–O theory quantifies the oscillator strength of electric dipole transitions in terms of set of three parameters (Ω_2, Ω_4 and Ω_6). J–O theory is extensively utilized in designing and optimizing optical materials for application in various optical devices like sensors and lasers etc.[56] The absorption profile of TbA, TbM and TbD complexes in liquid state using DCM solvent were also recorded in the near-infrared region i.e. lower energy region from 900 to 2900 nm. Here, the spectra of TbM and TbD are presented as TbA showed similar spectra as that of TbM with a little less intensity. Obtained absorption profiles present parity-forbidden but spin allowed sharp, narrow f–f absorption peaks arising from $^7F_6$ ground state (G. S.) to multiple excited states (E. S.) of Tb(III) ion. The optical absorption profile of these complexes displayed a total of 5 transitions originating from $^7F_6$ ground state of Tb(III) ion. These are appeared at 1671 nm, 1905 nm, 1979 nm, 2148 nm and 2703 nm corresponding to transition towards $^7F_0$, $^7F_1$, $^7F_2$, $^7F_3$ and $^7F_4$ states, respectively. J–O calculations were performed on obtained NIR absorption data for the determination of J–O parameters (Ω_2, Ω_4, Ω_6). These bands were assigned according to the work reported by Carnall and coworkers.[57] The intensity of these absorption peaks can be stated in terms of oscillator strength which is calculated using eqn (4).[58]

$$f_{\text{exp.}} = \frac{2.303mc^2}{N_A\pi e^2}\int \varepsilon(\bar{v})\cdot d\bar{v} = 4.319\times10^{-9}\left[\text{mol cm}^2\ 1^{-1}\right]\int\varepsilon(\bar{v})\cdot d\bar{v} \quad (4)$$

Here, molar absorptivity is expressed as ε and $\varepsilon(\bar{v})$ signifies molar absorptivity at respective wavenumber ($\bar{v}$) in cm^{-1}. Its value can be obtained by using area under the particular transition from the graph displayed in Fig. 10. The strength of electric dipole transitions originating from ground state i.e. $^7F_6$ is determined using eqn (5).[58]

$$f_{\text{calc.}} = \frac{8\pi^2 mc}{3h\lambda(2J+1)n^2}\frac{n(n^2+2)^2}{9}\sum_{t=2,4,6}\Omega_t\left|\langle\phi_J|U^t|\phi'_J\rangle\right|^2 \quad (5)$$

In the above relation, the terms π, m, c, h adhere to their conventional meanings. Here, λ and $(2J+1)$ signifies wavelength corresponding to absorption peak and spin multiplicity of ground J level and n represents refractivity index. Irreducible reduced matrix element is expressed as $\|U_t\|^2$ where t could be 2, 4 and 6. It acquires rank for intermediate coupling for transition between ground and excited electronic state and it remains unaffected by the coordinated ligand donors. Its numeric values were taken from Carnall et al.[59] Judd–Ofelt theory give details of both electric and magnetic dipole (MD) transitions but magnetic transitions are almost insignificant for the calculation of oscillator strength. Thereby, only electric dipole transitions are employed for determination of oscillator strength. The obtained

Table 7 Oscillator strength (exp. and calcd.) and J–O-parameter of TbA, TbM and TbD

Transitions	TbA		TbM		TbD	
$^7F_6 \rightarrow$	$f_{\text{exp.}}$	$f_{\text{calc.}}$	$f_{\text{exp.}}$	$f_{\text{calc.}}$	$f_{\text{exp.}}$	$f_{\text{calc.}}$
$^7F_0$	1.21	1.31	1.25	1.32	1.15	1.29
$^7F_1$	0.60	0.92	0.63	0.97	0.58	0.86
$^7F_2$	1.07	0.98	1.11	1.04	1.09	0.92
$^7F_3$	1.03	0.99	1.09	1.03	0.99	1.01
$^7F_4$	0.84	0.82	0.89	0.88	0.78	0.78
Ω_2 ($\times10^{20}$ cm^2)	6.075	—	6.124	—	6.007	—
Ω_4 ($\times10^{20}$ cm^2)	0.941	—	1.527	—	0.351	—
Ω_6 ($\times10^{20}$ cm^2)	3.817	—	4.114	—	3.542	—

results for calculated and experimental oscillator strength are concised in Table 7. Already reported studies have shown good correlation of absorption with $f_{\text{calc.}}$. Hence, the intensity variable (Ω_2, Ω_4, Ω_6) is estimated by equating both, calculated and experimental oscillator strength as presented in eqn (6).[58]

$$f_{\text{exp}}\leftrightarrow f_{\text{calc}} = \frac{8\pi^2 mc}{3h\lambda(2J+1)n^2}\frac{n(n^2+2)^2}{9}\left[\left(\Omega_2|\langle\phi_J|U^2|\phi'_J\rangle|^2\right)\right.$$
$$\left.+\left(\Omega_4|\langle\phi_J|U^4|\phi'_J\rangle|^2\right)+\left(\Omega_6|\langle\phi_J|U^6|\phi'_J\rangle|^2\right)\right] \quad (6)$$

The intensity parameters (Ω_2, Ω_4, Ω_6) for complexes TbM and TbD are presented in Table 7. The order followed by J–O parameters for these complexes is found to be $\Omega_2 > \Omega_6 > \Omega_4$. The largest numeric value obtained for Ω_2 in comparison to other intensity parameters (Ω_4, Ω_6) in TbM and TbD is indicating the presence of a covalent bond between M and O atoms, along with a markedly non-symmetric surrounding and a robust crystal field strength surrounding the Tb^{3+} ion. Additionally, the J–O parameters Ω_6 and Ω_4 provide comprehensive insights into the structural rigidity and viscosity of terbium complexes.[60] Radiative transition probability is an important feature to evaluate the amount of energy emitted by the compounds on irradiation with UV-rays. This variable is estimated by utilizing J–O parameters. The transition probability of the emission transitions from excited state to ground state of Tb^{3+} ion was determined by the eqn (7).[61]

$$A_{\text{rad.}} = \frac{64e^2\pi^4}{3h(2J+1)\lambda^3}\frac{n(n^2+2)^2}{9}[S_{\text{ED}}+S_{\text{MD}}] \quad (7)$$

In the above expression, strength of electrically and magnetically dipole lines are designated by S_{ED}, S_{MD} of each transition, respectively. S_{MD} is ignored in the estimation to obtain the equation given below (eqn (8)).[58]

$$A_{\text{rad.}} = \frac{64e^2\pi^4}{3h(2J+1)\lambda^3}\frac{n(n^2+2)^2}{9}S_{\text{ED}} \quad (8)$$

The expression for electric dipole line strength (S_{ED}) is given below in eqn (9).[58]

$$S_{\text{ED}} = \sum_{t=2,4,6}\left(\Omega_t|\langle\phi_J|U^t|\phi'_J\rangle|^2\right) \quad (9)$$

Table 8 Unified radiative properties of TbA, TbM and TbD

	TbA	TbM (solid)	TbD (solid)	$A_{rad.}$ (JJ′) (TbA)	(TbM)	(TbD)
$\beta(^5D_4$ to $^7F_6)$	0.09 (0.101)	0.180 (0.182)	0.151 (0.149)	77.47	89.57	97.62
$^7F_5$	0.875 (0.868)	0.602 (0.590)	0.507 (0.510)	265.77	342.85	295.47
$^7F_4$	0.027 (0.031)	0.100 (0.107)	0.109 (0.111)	31.88	24.78	32.13
$^7F_3$	0.006 (0.009)	0.116 (0.016)	0.232 (0.229)	29.13	35.96	46.52

Table 9 Radiative properties of TbA, TbM and TbD

Parameter	TbA	TbM	TbD
$A_{rad.}$ (total) (ms^{-1})	2.100	1.824	2.638
$A_{nrad.}$ (ms^{-1})	6.731	0.3219	0.0942
$\tau_{exp.}$ (ms)	0.103	0.466	0.366
$\tau_{rad.}$ (ms)	0.476	0.548	0.379

The matrix values utilized in the computation are drawn from ref. 62, while the resultant radiative metrics are detailed in Table 8. Subsequently, radiative decay time of the TbM and TbD could be examined through the inverse of the overall radiative rate.[58] The overall radiative-probability is defined as the summation of the probabilities of each transition originating from the lowest excited state ($^5D_4$) in the emission profile. Data for A_{rad} (total radiative), A_{nrad} (nonradiative) and τ_{rad} (radiative time) are concised in Table 9. These aforementioned variables exhibit higher values for TbD due to the inclusion of an additional metal center. Both the metal centers contribute towards the radiative relaxation, thereby enhancing the luminescence of ternary complexes.

5.6 Thermal characterization

The thermal stability of lanthanide (Ln) complexes is a crucial factor for their use in Ln-based OLEDs.[63] The thermal stability of the synthesized complexes was assessed by using thermogravimetric (TGA) analysis over a broad temperature range (RT to 750 °C). The thermograms of complexes TbM and TbD are shown in Fig. 11, displayed a two-step weight loss. For TbM, no significant weight loss occurred up to 154 °C, indicating that all the ligands remain coordinated to the Tb^{3+} ion up to this point. Between 154 °C and 316 °C, TbM showed a mass loss of approximately 12.39% (theor. = 16.60%), corresponding to the elimination of two bonded pyrazine molecules. The subsequent detachment of three TFPB ligands occurred between 298 °C and 729 °C, resulting in a 70.16% mass loss (theor. = 67.23%), leaving metal oxide (Tb$_2$O$_3$) as the final residue. For TbD, the TGA curve showed a total mass loss of 80.50% (theoretical = 81.53%) within the 164 °C to 706 °C range. The first minor mass loss of ~4.84% (theoretical = 4.74%) from 164 °C to 305 °C corresponded to the elimination of a spacer pyrazine molecule. The major decomposition occurred from 305 °C, with a mass loss of 75.43% (theoretical = 76.79%), corresponding to the detachment of TFPB ligands between 305 °C and 704 °C. The mononuclear Tb-complex exhibited lower thermal stability. The final residue for TbD was attributed to Tb$_2$O$_3$, as indicated by the weight loss calculations. Similarly, the thermal curve for TbA displayed a two-step weight loss, with a bending point at ~100 °C due to the dissociation of two water molecules, resulting in a 4.59% weight loss (theor. = 4.28%). Beyond this temperature, only TFPB ligands remained coordinated to the
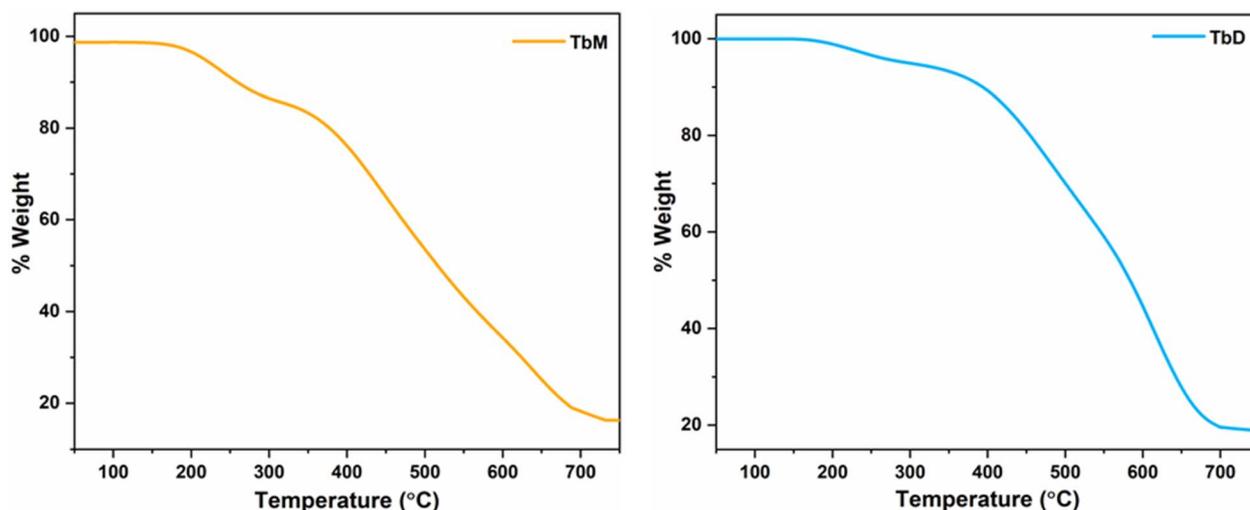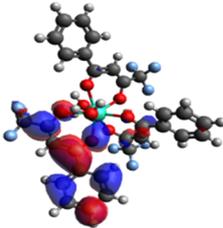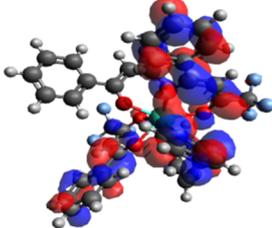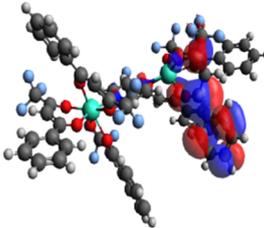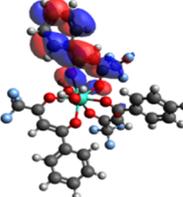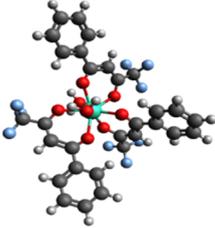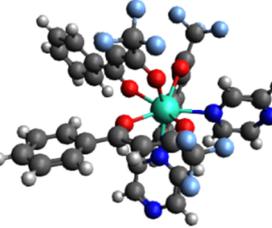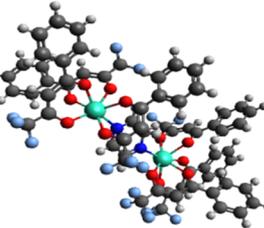

Fig. 11 TGA curves of TbM and TbD.

Tb^{3+} ion. The TGA curve for TbA showed an 79.47% mass loss (theor. = 77.15%) between 103 °C and 652 °C, corresponding to the elimination of three bonded TFPB ligands, with metal oxide (Tb_2O_3) as the final residue, resulting in an overall weight loss of 84.06% (theor. = 81.43%).

5.7 Computational modelling

Molecular geometries of synthesized complexes were generated in Avogadro software and energy minimization was done *via* auto optimization tools.[64] Geometry optimization of these large molecules was done using BP/def2-SVP (DFT level) and def2-SVP

(basis set).[65] As the f-orbitals are deeply buried in the shell and do not play a significant role in metal ligand bonds, thus, we have used large-core quasi-relativistic effective core potential. DFT calculations were carried out by using ORCA and Avogadro software.[66–68] Following complete energy minimization (dE = 0) the optimized file is used as input for further calculations in ORCA software[69] which resulted in generation of an ORCA output file which facilitates the representation of FMOs (Frontier Molecular Orbitals) in Avogadro software. Structures and energy of various molecular orbitals *viz.*, HOMO−1, HOMO, LUMO and LUMO+1 were estimated (Table 10). The energy

Table 10 Structure and energy levels of TbA–TbD

	TbA	TbM	TbD
LUMO+1	(−2.101 eV)	(−1.789 eV)	(−1.969 eV)
LUMO	(−3.181 eV)	(−3.244 eV)	(−3.049 eV)
HOMO	(−6.567 eV)	(−6.671 eV)	(−6.458 eV)
HOMO−1	(−7.141 eV)	(−7.999 eV)	(−7.032 eV)
Complex	TbA	TbM	TbD
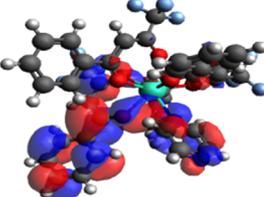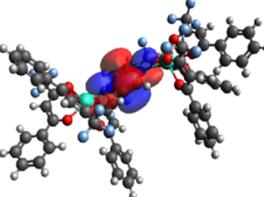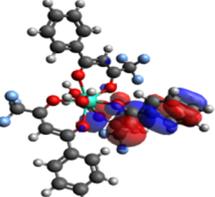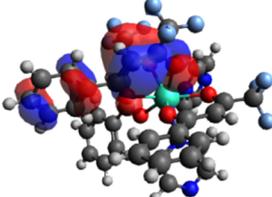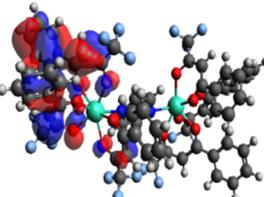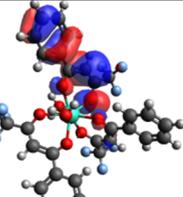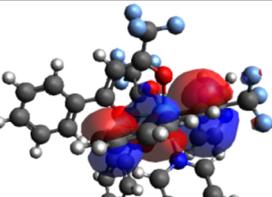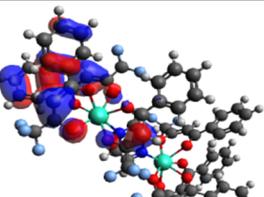
difference between HOMO and LUMO levels provide theoretical band gap values. These values show excellent concordance with experimentally analyzed band gap data (*via* CV analysis and UV analysis). These results ensure the accuracy and reliability of employed computational results. Values within 3–4 eV range make them potential candidate for use in optoelectronic applications. With the relation proposed by Koopmans depicted in eqn (10), the ionization energy (IE) is related to energy of HOMO level and electron affinity (EA) to the energy of LUMO level respectively. This allowed the quantification of various global reaction parameters.[70] Derived from DFT analysis, global reactivity descriptors include chemical hardness (η), ionization potential (μ), electronegativity (χ), Fukui functions and softness (σ) (eqn (11)).[71] These descriptors offer detailed insights into the chemical stability and reactivity of the system, as well as its tendency to accept or donate electrons during chemical reactions. They assist in the reaction design and optimization by identifying reactive sites, predicting reaction rates and assessing the likelihood of undesired side reactions. These global reactivity parameters are concised in Table 11.

$$\text{IE} = -E_{\text{HOMO}}, \ \text{EA} = -E_{\text{LUMO}} \tag{10}$$

$$\chi = \frac{\text{IE} + \text{EA}}{2}, \ \eta = \frac{\text{IE} - \text{EA}}{2}, \ \sigma = \frac{1}{\eta}, \ \mu = -\chi \tag{11}$$

Among the three synthesized complexes, TbM exhibits the highest ionization energy of 6.671 eV, while TbA and TbD have slightly lower ionization energies of 6.567 and 6.458 eV, respectively. Similarly, TbM has the greatest electron affinity of 3.244 eV, compared to 3.181 eV for TbA and 3.049 eV for TbD. Using these ionization energy (IE) and electron affinity (EA) values, the electronegativity of the complexes was calculated according to Mulliken's scale (eqn (11)). The results indicate that TbM has the highest electronegativity at 4.957 eV, followed by TbA with 4.874 eV and TbD with the lowest at 4.753 eV. The chemical hardness, derived from IE and EA values, reveals that TbA, TbM and TbD have hardness values of 1.693, 1.713 and 1.704 units, respectively. This indicates that TbM is the chemically most stable complex, whereas TbA is the least stable, as chemical hardness correlates with stability. In terms of chemical softness, TbA has the highest value at 0.590, while TbM has the lowest at 0.583, with TbD at 0.586. This suggests that TbM is the least reactive and TbA is the most reactive complex, as softness is an indicator of chemical reactivity. Overall, these findings demonstrate that the water-coordinated complex (binary complex/TbA) is the least stable and most reactive, while the mononuclear complex is the least reactive and most stable among the three prepared complexes.

Table 11 Molecular parameters of synthesized complexes

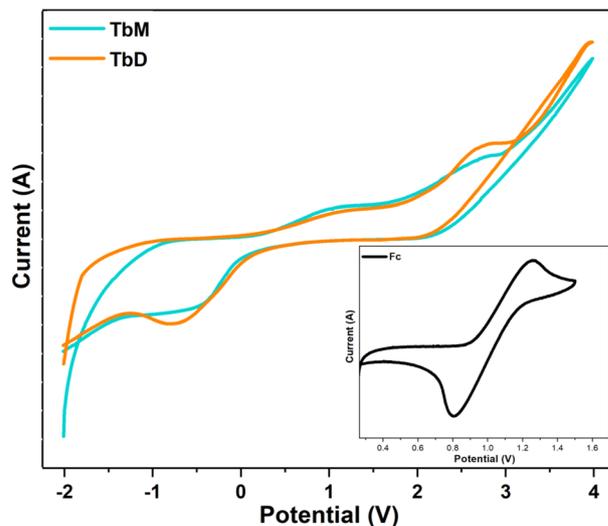| Complex	IE	EA	χ	η	σ	μ
TbA	6.567	3.181	4.874	1.693	0.590	−4.874
TbM	6.671	3.244	4.957	1.713	0.583	−4.957
TbD	6.458	3.049	4.753	1.704	0.586	−4.753

Fig. 12 (*I*–*V*) plots of synthesized complexes.

Table 12 Redox potential and electronic band gap values of TbA–TbD

Compound	$E_{\text{ox.}}$ (V)	$E_{\text{red.}}$ (V)	E_{HOMO} (eV)	E_{LUMO} (eV)	E_{g}^{a} (eV)
TbA	2.7790	−0.7168	−6.5490	−3.0532	3.4958
TbM	2.8079	−0.6186	−6.5779	−3.1514	3.4265
TbD	2.7067	−0.7066	−6.4767	−3.0634	3.4133

5.8 Cyclo-voltammetry analysis

An electrochemical investigation was performed on synthesized complexes (TbA, TbM and TbD) *via* cyclic voltammetry and the resulting cyclic curves are shown in the Fig. 12. The CV plots were extensively examined and the redox potentials for the complexes were calculated and unified in Table 12. The energy of HOMO (Highest Occupied Molecular Orbital) and LUMO (Lowest Unoccupied Molecular Orbital) levels was calculated using the below-mentioned two equations (eqn (12) and (13)), as reported by N. G. Tsierkezos (Table 12).[72]

$$E_{\text{HOMO}} = -[E_{\text{ox}} - E_{1/2(\text{ferrocene})} + 4.8] \text{ eV} \tag{12}$$

$$E_{\text{LUMO}} = -[E_{\text{red}} - E_{1/2(\text{ferrocene})} + 4.8] \text{ eV} \tag{13}$$

Mononuclear complexes have somewhat larger electronic energy gap values (E_{g}^{a}) compared to dinuclear complexes (Table 12). The estimated energy of HOMO–LUMO levels is found to be comparable to that obtained from computational calculations. The electronic band gap is quite similar to the optical band gap and DFT derived band gap.

6. Conclusions

Two complexes featuring a pyrazine spacer were successfully synthesized, resulting in binuclear complex and its binary and ternary mononuclear counterparts. Signals for pyrazine protons

in Proton NMR spectra and a significant increase in the intensity of hypersensitive transitions of Tb(III) ions, alongside elemental analysis, strongly support the formation of desired dinuclear complexes. The bonding of bridging moiety not only amplifies the intensity of incident UV-absorption but also meets the high coordinative requirement of the trivalent ion, thereby enhancing coordination saturation and thermal stabilities, as evidenced by thermogravimetric results. The agreement among the band gap values obtained from optical, electronic and computational techniques, all within the 3.40–3.50 eV range, suggests their potential to be utilized as semiconducting components in optoelectronic devices, such as organic light-emitting diodes (OLEDs) and laser diodes. Global reactivity parameters show that water-coordinated complex (binary complex/TbA) is the least stable ($\eta = 1.693$) and most reactive ($\sigma = 0.590$), while the mononuclear complex (TbM) is the least reactive ($\sigma = 0.583$) and most stable ($\eta = 1.713$) among the three prepared complexes. Emission spectral analysis of these Tb-complexes revealed a transition from green to blue to pink to white emission, in moving from solid to solution states, with a broad ligand-based band. Enhanced emission intensity in solid state compared to solution, leading to pure and intense emission, as confirmed by CIE coordinates. Furthermore, the white emission observed from these complexes in solution phase indicates their potential for application in white light-emitting diodes (wLEDs). Additionally, Judd–Ofelt parameters were calculated to validate experimental findings against theoretical calculations. Higher radiative transition probability of $^5D_4 \rightarrow {}^7F_5$ transition in TbM from J–O analysis validates the emission intensities observed in PL spectra. These prepared complexes hold promise for various applications such as OLEDs, optical amplification, laser systems or medical diagnostics.

Data availability

The authors affirm that the information/data of this research article is available inside the article.

Author contributions

Vandana Aggarwal = data curation, writing – original draft; Devender Singh = writing – review & editing and supervision; Shri Bhagwan = investigation; Raman Kumar Saini = visualization; Komal Jakhar = validation; Sumit Kumar = resources; Parvin Kumar = software; Jayant Sindhu = formal analysis.

Conflicts of interest

The authors declare that they have no conflict of interest.

Acknowledgements

References

1 A. Hooda, D. Singh, A. Dalal, K. Nehra, S. Kumar, R. S. Malik, R. Kumar and P. Kumar, Optical, electrochemical and photophysical analyses of heteroleptic luminescent Ln (III) complexes for lighting applications, *RSC Adv.*, 2023, **13**, 9033–9045, DOI: **10.1039/D3RA00214D**.

2 K. Nehra, A. Dalal, A. Hooda, S. Bhagwan, R. K. Saini, B. Mari, S. Kumar and D. Singh, Lanthanides β-diketonate complexes as energy-efficient emissive materials: A review, *J. Mol. Struct.*, 2022, **1249**, 131531, DOI: **10.1016/j.molstruc.2021.131531**.

3 K. Nehra, A. Dalal, A. Hooda, R. K. Saini, D. Singh, S. Kumar, R. S. Malik, R. Kumar and P. Kumar, Synthesis of green emissive terbium (III) complexes for displays: Optical, electrochemical and photoluminescent analysis, *Luminescence*, 2023, **38**, 56–63, DOI: **10.1002/bio.4423**.

4 D. Singh, K. Nehra, R. K. Saini, A. Dalal, S. Bhagwan, K. Singh, A. P. Simantilleke and S. Kumar, Luminescence intensification of terbium (III) ion complexes with dipivaloylmethane (tmhd) and monodentate auxiliary ligands, *Optik*, 2020, **206**, 164338, DOI: **10.1016/j.ijleo.2020.164338**.

5 M. Cui, A. L. Wang, C. L. Gao, L. Zhou, T. Wu, S. Fang, H. P. Xiao, F. C. Li and X. L. Li, Two homochiral Eu(III) and Sm(III) enantiomeric pairs showing circularly polarized luminescence, photoluminescence and triboluminescence, *Dalton Trans.*, 2021, **50**, 1007–1018, DOI: **10.1039/D0DT03576A**.

6 A. Dalal, K. Nehra, A. Hooda, P. Kumar, D. Singh, S. Kumar, R. Kumar and P. Kumar, Red emissive β-diketonate Ln (III) complexes for displays: Preparation, spectroscopic and optical investigations, *Optik*, 2023, **276**, 170648, DOI: **10.1016/j.ijleo.2023.170648**.

7 X. L. Li, A. Wang, Y. Li, C. Gao, M. Cui, H. P. Xiao and L. Zhou, Two Chiral Yb(III) Enantiomeric Pairs with Distinct Enantiomerically Pure N-Donor Ligands Presenting Significant Differences in Photoluminescence, Circularly Polarized Luminescence, and Second-Harmonic Generation, *Inorg. Chem.*, 2023, **62**, 4351–4360, DOI: **10.1021/acs.inorgchem.3c00106**.

8 K. Nehra, A. Dalal, A. Hooda, D. Singh and S. Kumar, Exploration of newly synthesized red luminescent material of samarium for display applications, *Inorg. Chem. Commun.*, 2022, **139**, 109361, DOI: **10.1016/j.inoche.2022.109361**.

9 Y. Peng, T. Wang, C. Gao, F. Li and X. L. Li, Two chiral lanthanide Pr(III) and Ho(III) complexes:NIR luminescence and nonlinear optical properties, *CrystEngComm*, 2024, **26**, 3867–3873, DOI: **10.1039/D4CE00421C**.

10 K. Nehra, A. Dalal, A. Hooda, P. Kumar, D. Singh, S. Kumar, R. S. Malik and P. Kumar, Luminous terbium and samarium complexes with diacetylmethane and substituted 1, 10-phenanthroline derivatives for display applications: Preparation and optoelectronic investigations, *J. Lumin.*, 2022, **249**, 119032, DOI: **10.1016/j.jlumin.2022.119032**.

11 X. L. Li, X. L. Zhang, M. Hu, C. Zhu, C. Chen and A. L. Wang, Homochiral mono-and dinuclear SmIII complexes showing the effect of nuclearity on their photophysical properties, *Polyhedron*, 2016, **111**, 94–100, DOI: **10.1016/j.poly.2016.03.043**.

12 K. Nehra, A. Dalal, A. Hooda, S. Singh and D. Singh, Computational and spectroscopic evaluation of 1, 10-phenanthroline based Eu (III) fluorinated β-diketonate complexes for displays, *J. Lumin.*, 2022, **251**, 119111, DOI: **10.1016/j.jlumin.2022.119111**.

13 A. Dalal, K. Nehra, A. Hooda, S. Singh, D. Singh and S. Kumar, Synthesis, optoelectronic and photoluminescent characterizations of green luminous heteroleptic ternary terbium complexes, *J. Fluoresc.*, 2022, **32**, 1019–1029, DOI: **10.1007/s10895-022-02920-7**.

14 P. Kumar, S. Singh, I. Gupta, K. Nehra, V. Kumar and D. Singh, Structural refinement and optical characteristics of single-phase $Gd_3Al_5O_{12}:Er^{3+}$ nanophosphors for luminescent applications, *J. Lumin.*, 2022, **252**, 119338, DOI: **10.1016/j.jlumin.2022.119338**.

15 J. H. Monteiro, Recent advances in luminescence imaging of biological systems using lanthanide (III) luminescent complexes, *Molecules*, 2020, **25**, 2089, DOI: **10.3390/molecules25092089**.

16 P. Kumar, D. Singh and I. Gupta, UV excitable $GdSr_2AlO_5$:Eu^{3+} red emitting nanophosphors: structure refinement, photoluminescence, Judd-Ofelt analysis and thermal stability for w-LEDs, *J. Alloys Compd.*, 2023, **966**, 171410, DOI: **10.1016/j.jallcom.2023.171410**.

17 V. Aggarwal, D. Singh, S. Bhagwan, R. K. Saini, K. Jakhar, R. S. Malik, P. Kumar and J. Sindhu, Exploring the Influence of Emissive Centers in Mono and Dinuclear Europium (III) Complexes for Advance Lighting Applications: Synthesis, Characterization and Computational Modelling, *J. Mol. Struct.*, 2024, 140841, DOI: **10.1016/j.molstruc.2024.140841**.

18 D. Singh, K. Singh, S. Bhagwan, R. K. Saini, R. Srivastava and I. Singh, Preparation and photoluminescence enhancement in terbium (III) ternary complexes with β-diketone and monodentate auxiliary ligands, *Cogent Chem.*, 2016, **2**, 1134993, DOI: **10.1080/23312009.2015.1134993**.

19 A. Hooda, A. Dalal, K. Nehra, D. Singh, S. Kumar, R. S. Malik and P. Kumar, Preparation and optical investigation of green luminescent ternary terbium complexes with aromatic β-diketone, *Chem. Phys. Lett.*, 2022, **794**, 139495, DOI: **10.1016/j.cplett.2022.139495**.

20 A. Hooda, K. Nehra, A. Dalal, S. Singh, R. K. Saini, S. Kumar and D. Singh, Terbium complexes of an asymmetric β-diketone: preparation, photophysical and thermal investigation, *Inorg. Chim. Acta*, 2022, **536**, 120881, DOI: **10.1016/j.ica.2022.120881**.

21 L. L. Cai, S. M. Zhang, Y. Li, K. Wang, X. M. Li, G. Muller, F. P. Liang, Y. T. Hu and G. X. Wang, Lanthanide nitrato complexes bridged by the bis-tridentate ligand 2, 3, 5, 6-tetra (2-pyridyl) pyrazine: Syntheses, crystal structures, Hirshfeld surface analyses, luminescence properties, DFT calculations, and magnetic behavior, *J. Lumin.*, 2021, **232**, 117835, DOI: **10.1016/j.jlumin.2020.117835**.

22 S. Viviani, A. Fratini and S. Swavey, The effect of the lanthanide contraction on coordination with the polyazine bridging ligand 2, 3-bis (2-pyridyl) pyrazine (dpp), *Inorg. Chem. Commun.*, 2012, **24**, 29–31, DOI: **10.1016/j.inoche.2012.07.035**.

23 K. Nehra, A. Dalal, A. Hooda, S. Singh, D. Singh, S. Kumar, R. S. Malik, R. Kumar and P. Kumar, Red luminous Eu (III) complexes: Preparation, spectral, optical and theoretical evaluation, *Inorg. Chim. Acta*, 2022, **539**, 121007, DOI: **10.1016/j.ica.2022.121007**.

24 A. Dalal, K. Nehra, A. Hooda, D. Singh, J. Dhankhar and S. Kumar, Fluorinated β-diketone-based Sm (III) complexes: spectroscopic and optoelectronic characteristics, *Luminescence*, 2022, **37**, 1328–1334, DOI: **10.1002/bio.4300**.

25 G. Qian-Ling, Z. Wen-Xiang, G. Rong, Y. Xi and W. Ru-Ji, Crystal Structure of Complex Tris (4,4,4-trifluoro-1-pheny1–1,3-butanedione)(1,10-phenanthroline) Europium (III), *Chin. J. Chem.*, 2003, **21**, 211–215, DOI: **10.1002/cjoc.20030210225**.

26 A. Hooda, D. Singh, A. Dalal, K. Nehra, S. Kumar, R. S. Malik, H. Sehrawat and P. Kumar, N-donor auxiliary ligand-based terbium (III) β-diketonates: Preparation and photophysical studies, *J. Lumin.*, 2023, **258**, 119828, DOI: **10.1016/j.jlumin.2023.119828**.

27 A. Hooda, K. Nehra, A. Dalal, S. Singh, S. Bhagwan, K. Jakhar and D. Singh, Preparation and photoluminescent analysis of Sm^{3+} complexes based on unsymmetrical conjugated chromophoric ligand, *J. Mater. Sci. Mater. Electron.*, 2022, **33**, 11132–11142, DOI: **10.1007/s10854-022-08089-w**.

28 A. Hooda, D. Singh, K. Nehra, S. Dalal, V. Aggarwal, S. Kumar, R. S. Malik and P. Kumar, Preparation and optical studies of octacoordinated luminescent complexes of Dy(III) derived from fluorinated β-diketone and heteroaromatic neutral ligands, *Inorg. Chim. Acta*, 2023, **556**, 121674, DOI: **10.1016/j.ica.2023.121674**.

29 R. Ilmi and K. Iftikhar, Pyrazine bridged Ln_2 (La, Nd, Eu and Tb) complexes containing fluorinated β-diketone, *Inorg. Chem. Commun.*, 2012, **20**, 7–12, DOI: **10.1016/j.inoche.2012.01.037**.

30 V. Aggarwal, D. Singh, A. Hooda, S. Malik, S. Dalal, S. Redhu, S. Kumar, R. S. Malik and P. Kumar, Comprehensive investigation of ternary dysprosium complexes for white light emission: Synthesis, spectroscopic and colorimetric analyses, *J. Lumin.*, 2024, 120555, DOI: **10.1016/j.jlumin.2024.120555**.

31 A. Ali, Z. Ahmed and K. Iftikhar, Heteroleptic samarium complexes with high quantum yields for temperature sensing applications, *Dalton Trans.*, 2024, **53**, 1105–1120, DOI: **10.1039/D3DT03160H**.

32 S. Malik, K. Jakhar, D. Singh, A. Hooda, K. Nehra, S. Kumar, R. S. Malik and P. Kumar, Near ultra-violet excitable Tb(III)-tris-hexafluoro-2,4-pentanedione complexes for OLEDs: Insights into the impact of ancillary ligands on

photoluminescent characteristics, *J. Mol. Struct.*, 2024, **1311**, 138334, DOI: **10.1016/j.molstruc.2024.138334**.

33 B. Klein and J. Berkowitz, Pyrazines. I. Pyrazine-N-oxides. Preparation and Spectral Characteristics, *J. Am. Chem. Soc.*, 1959, **81**, 5160–5166, DOI: **10.1021/ja01528a035**.

34 V. Aggarwal, D. Singh, A. Hooda, K. Nehra, K. Jakhar, S. Kumar, R. S. Malik and P. Kumar, Synthesis and photoluminescent analyses of ternary terbium(III) Tris-β-diketonate complexes: A systematic exploration, *J. Mater. Sci.: Mater. Electron.*, 2024, **35**, 568, DOI: **10.1007/s10854-024-12314-z**.

35 V. Aggarwal, D. Singh, A. Hooda, K. Nehra, S. Redhu, S. Kumar, R. S. Malik and P. Kumar, Design and spectroscopic study of samarium complexes with tunable photoluminescent properties, *J. Mol. Struct.*, 2024, **1311**, 138315, DOI: **10.1016/j.molstruc.2024.138315**.

36 V. Aggarwal, D. Singh, S. Redhu, S. Malik, S. Dalal, S. Kumar, R. S. Malik, P. Kumar and J. Sindhu, Design and photophysical characterization of dinuclear lanthanide complexes incorporating spacer ligands along with their mononuclear analogues: A comparative study, *Opt. Mater.*, 2024, **155**, 115833, DOI: **10.1016/j.optmat.2024.115833**.

37 A. Dalal, K. Nehra, A. Hooda, D. Singh, K. Jakhar and S. Kumar, Preparation and photoluminescent characteristics of green Tb (III) complexes with β-diketones and N donor auxiliary ligands, *Inorg. Chem. Commun.*, 2022, **139**, 109349, DOI: **10.1016/j.inoche.2022.109349**.

38 E. Berti, A. Caneschi, C. Daiguebonne, P. Dapporto, M. Formica, V. Fusi, L. Giorgi, A. Guerri, M. Micheloni, P. Paoli and R. Pontellini, Ni (II), Cu (II), and Zn (II) Dinuclear Metal Complexes with an Aza−Phenolic Ligand: Crystal Structures, Magnetic Properties, and Solution Studies, *Inorg. Chem.*, 2003, **42**, 348–357, DOI: **10.1021/ic0204070**.

39 K. Nehra, A. Dalal, A. Hooda, K. Jakhar, D. Singh and S. Kumar, Preparation, optoelectronic and spectroscopic analysis of fluorinated heteroleptic samarium complexes for display applications, *Inorg. Chim. Acta*, 2022, **537**, 120958, DOI: **10.1016/j.ica.2022.120958**.

40 A. Hooda, K. Nehra, A. Dalal, S. Singh, S. Bhagwan, K. Jakhar and D. Singh, Preparation and photoluminescent analysis of Sm^{3+} complexes based on unsymmetrical conjugated chromophoric ligand, *J. Mater. Sci. Mater. Electron.*, 2022, **33**, 11132–11142, DOI: **10.1007/s10854-022-08089-w**.

41 K. Nehra, A. Dalal, A. Hooda, S. Singh, D. Singh and S. Kumar, Spectroscopic and optical investigation of 1, 10-phenanthroline based Tb(III) β-diketonate complexes, *Inorg. Chim. Acta*, 2022, **536**, 120860, DOI: **10.1016/j.ica.2022.120860**.

42 F. F. Silva, F. L. Menezes and L. L. Luz, Supramolecular luminescent hydrogels based on β-amino acid and lanthanide ions obtained by self-assembled hydrothermal reactions, *New J. Chem.*, 2014, **38**, 893–896, DOI: **10.1039/C3NJ01560B**.

43 S. Redhu, D. Singh, A. Hooda, A. Dalal, K. Jakhar, S. Kumar, R. S. Malik, P. Kumar and J. Sindhu, Examination of the spectroscopic characteristics of bright green emitting, octa

coordinated luminescent terbium(III) complexes, *Polyhedron*, 2024, **253**, 116926, DOI: **10.1016/j.poly.2024.116926**.

44 S. Redhu, D. Singh, A. Hooda, S. Malik, V. Aggarwal, S. Dalal, S. Kumar, R. S. Malik and P. Kumar, Photoluminescence tuning of terbium tris-1,1,1-trifluoro-5,5-dimethyl-2,4-hexanedione complexes: Synthesis, spectroscopic, thermal and electrochemical analyses, *J. Lumin.*, 2024, **271**, 120588, DOI: **10.1016/j.jlumin.2024.120588**.

45 V. Aggarwal, D. Singh, S. Bhagwan, R. K. Saini, K. Jakhar, R. S. Malik, P. Kumar and J. Sindhu, Exploring the Influence of Emissive Centers in Mono and Dinuclear Europium (III) Complexes for Advance Lighting Applications: Synthesis, Characterization and Computational Modelling, *J. Mol. Struct.*, 2024, 140841, DOI: **10.1016/j.molstruc.2024.140841**.

46 P. Kumar, D. Singh, I. Gupta, S. Singh, V. Kumar, H. Kumar and S. K. Chhikara, Cool green light emitting $GdAlO_3$: Tb^{3+} perovskite nanomaterials: Crystal structure and spectroscopic characteristics for advance display appliances, *Inorg. Chem. Commun.*, 2022, **145**, 110064, DOI: **10.1016/j.inoche.2022.110064**.

47 J. Kommandeur, W. A. Majewski, W. L. Meerts and D. W. Pratt, Pyrazine: An "exact" solution to the problem of radiationless transitions, *Annu. Rev. Phys. Chem.*, 1987, **38**, 433–462, DOI: **10.1146/annurev.pc.38.100187.002245**.

48 R. L. Tranquilin, L. X. Lovisa, C. R. Almeida, C. A. Paskocimas, M. S. Li, M. C. Oliveira, L. Gracia, J. Andres, E. Longo, F. V. Motta and M. R. Bomio, Understanding the white-emitting $CaMoO_4$ Co-doped Eu^{3+}, Tb^{3+}, and Tm^{3+} phosphor through experiment and computation, *J. Phys. Chem. C*, 2019, **123**, 18536–18550, DOI: **10.1021/acs.jpcc.9b04123**.

49 W. S. Lo, J. Zhang, W. T. Wong and G. L. Law, Highly Luminescent SmIII Complexes with Intraligand Charge-Transfer Sensitization and the Effect of Solvent Polarity on Their Luminescent Properties, *Inorg. Chem.*, 2015, **54**, 3725–3727, DOI: **10.1021/acs.inorgchem.5b00331**.

50 S. K. Gupta, C. Reghukumar and R. M. Kadam, Eu^{3+} local site analysis and emission characteristics of novel $Nd_2Zr_2O_7$:Eu phosphor: insight into the effect of europium concentration on its photoluminescence properties, *RSC Adv.*, 2016, **6**, 53614–53624, DOI: **10.1039/C6RA11698A.**

51 Z. Yonghui, C. Mindong, G. U. Shengli, X. U. Jianqiang, G. Guizhi, K. O. Qinggang, H. Gang, L. Jun, M. A. Yan, G. U. Yan and Y. Zheng, Photoluminescence properties of dinuclear lanthanide complexes in visible and near-infrared region, *J. Rare Earths*, 2010, **28**, 660–665, DOI: **10.1016/S1002-0721(09)60174-5**.

52 H. Y. Li, J. Wu, W. Huang, Y. H. Zhou, H. R. Li, Y. X. Zheng and J. L. Zuo, Synthesis and photoluminescent properties of five homodinuclear lanthanide (Ln^{3+} = Eu^{3+}, Sm^{3+}, Er^{3+}, Yb^{3+}, Pr^{3+}) complexes, *J. Photochem. Photobiol., A*, 2009, **208**, 110–116, DOI: **10.1016/j.jphotochem.2009.09.003**.

53 K. Nehra, A. Dalal, A. Hooda, S. Bhagwan, K. Jakhar, D. Singh, R. S. Malik, S. Kumar and B. Rathi, Synthesis, thermal and photoluminescence investigation of Tb (III) β-

diketonates with 1,10-phenanthroline derivatives, *J. Lumin.*, 2022, **251**, 119233, DOI: **10.1016/j.jlumin.2022.119233**.

54 W. A. Dar and K. Iftikhar, Phase controlled colour tuning of samarium and europium complexes and excellent photostability of their PVA encapsulated materials, Structural elucidation, photophysical parameters and the energy transfer mechanism in the Eu^{3+} complex by Sparkle/PM3 calculations, *Dalton Trans.*, 2016, **45**, 8956–8971, DOI: **10.1039/C6DT00549G**.

55 M. J. Beltrán-Leiva, D. Páez-Hernández and R. Arratia-Pérez, Theoretical determination of energy transfer processes and influence of symmetry in Lanthanide (III) complexes: Methodological considerations, *Inorg. Chem.*, 2018, **57**, 5120–5132, DOI: **10.1021/acs.inorgchem.8b00159**.

56 K. Nehra, A. Dalal, A. Hooda, D. Singh, S. Kumar, R. S. Malik and P. Kumar, Influence of coordinating environment on photophysical properties of UV excited sharp red emitting material: Judd Ofelt analysis, *J. Photochem. Photobiol. A: Chem.*, 2022, **430**, 113999, DOI: **10.1016/j.jphotochem.2022.113999**.

57 W. T. Carnall, P. R. Fields and K. Rajnak, *J. Chem. Phys.*, 1968, **1968**, 49.

58 P. Kumari, V. Lather, P. Ahlawat, M. Kumar and R. Kumar, Lasing properties, Judd-Ofelt and band gap investigation of cool green emanating Tb^{3+} complexes for solid and solution state luminescence, *Opt. Mater.*, 2024, **147**, 114677, DOI: **10.1016/j.optmat.2023.114677**.

59 W. T. Carnall, P. R. Fields and K. Rajnak, Spectral intensities of the trivalent lanthanides and actinides in solution. II. Pm^{3+}, Sm^{3+}, Eu^{3+}, Gd^{3+}, Tb^{3+}, Dy^{3+}, and Ho^{3+}, *J. Chem. Phys.*, 1968, **49**, 4412–4423, DOI: **10.1063/1.1669892**.

60 J. H. Monteiro, I. O. Mazali and F. A. Sigoli, Determination of Judd-Ofelt intensity parameters of pure samarium (III) complexes, *J. Fluoresc.*, 2011, **21**, 2237–2243, DOI: **10.1007/s10895-011-0928-x**.

61 B. C. Jamalaiah, J. S. Kumar, A. M. Babu, T. Suhasini and L. R. Moorthy, Photoluminescence properties of Sm^{3+} in LBTAF glasses, *J. Lumin.*, 2009, **129**, 363–369, DOI: **10.1016/j.jlumin.2008.11.001**.

62 A. Aebischer, F. Gumy and J. C. Bünzli, Intrinsic quantum yields and radiative lifetimes of lanthanide tris (dipicolinates), *Phys. Chem. Chem. Phys.*, 2009, **11**, 1346–1353, DOI: **10.1039/B816131C**.

63 S. Dalal, D. Singh, A. Dalal, A. Hooda, S. Kumar, R. S. Malik, P. Kumar and J. Sindhu, Green emissive Tb (III) complexes based on photosensitizing antenna: Synthesis and optoelectronic analysis, *Mater. Sci. Semicond. Process.*, 2024, **177**, 108370, DOI: **10.1016/j.mssp.2024.108370**.

64 M. D. Hanwell, D. E. Curtis, D. C. Lonie, T. Vandermeerschd, E. Zurek and G. R. Hutchison Avogadro, An advanced semantic chemical editor, visualization, and analysis platform, *J. Cheminf.*, 2012, **4**, 1, DOI: **10.1186/1758-2946-4-17**.

65 F. Weigend and R. Ahlrichs, Balanced basis sets of split valence, triple zeta valence and quadruple zeta valence quality for H to Rn: Design and assessment of accuracy, *Phys. Chem. Chem. Phys.*, 2005, **7**, 3297–3305, DOI: **10.1039/B508541A**.

66 M. Dolg, H. Stoll, A. Savin and H. Preuss, Energy-adjusted pseudopotentials for the rare earth elements, *Theor. Chim. Acta*, 1989, **75**, 173–194, DOI: **10.1007/BF00528565**.

67 M. Dolg, H. Stoll and H. Preuss, Energy-adjusted *ab initio* pseudopotentials for the rare earth elements, *J. Chem. Phys.*, 1989, **90**, 1730–1734, DOI: **10.1063/1.456066**.

68 X. Cao, M. Dolg and H. Stoll, Valence basis sets for relativistic energy-consistent small-core actinide pseudopotentials, *J. Chem. Phys.*, 2003, **118**, 487–496, DOI: **10.1063/1.1406535**.

69 F. Neese, The ORCA program system, *Rev.:Comput. Mol. Sci.*, 2012, **2**, 73, DOI: **10.1002/wcms.81**.

70 T. Koopmans, Über die Zuordnung von Wellenfunktionen und Eigenwertenzu den EinzelnenElektronenEines Atoms, *Physica*, 1934, **1**, 104–113, DOI: **10.1016/S0031-8914(34)90011-2**.

71 R. Vijayaraj, V. Subramanian and P. K. Chattaraj, Comparison of global reactivity descriptors calculated using various density functionals: a QSAR perspective, *J. Chem. Theor. Comput.*, 2009, **5**, 2744, DOI: **10.1021/ct900347f**.

72 K. Nehra, A. Dalal, A. Hooda, D. Singh, R. S. Malik and S. Kumar, Spectroscopic and optoelectronic investigations of 3,8-Bis(3,4-(ethylenedioxy)thien-2-yl)-1,10-phenanthroline, *J. Mater. Sci. Mater. Electron.*, 2022, **33**, 115–125, DOI: **10.1007/s10854-021-07268-5**.